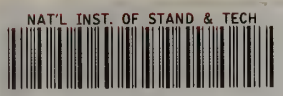

Fire Induced Flows Through Room Openings - Flow Coefficients

U.S. DEPARTMENT OF COMMERCE
National Bureau of Standards
National Engineering Laboratory
Center for Fire Research
Washington, DC 20234

March 1984

Sponsored in part by:
Armstrong World Industries
Lancaster, PA 17604

NBSIR 83-2801

FIRE INDUCED FLOWS THROUGH ROOM OPENINGS - FLOW COEFFICIENTS

K. D. Steckler
H. R. Baum
J. G. Quintiere

U.S. DEPARTMENT OF COMMERCE
National Bureau of Standards
National Engineering Laboratory
Center for Fire Research
Washington, DC 20234

March 1984

Sponsored in part by:
Armstrong World Industries
Lancaster, PA 17604

U.S. DEPARTMENT OF COMMERCE, Malcolm Baldrige, *Secretary*
NATIONAL BUREAU OF STANDARDS, Ernest Ambler, *Director*

TABLE OF CONTENTS

	Page
LIST OF FIGURES	iv
LIST OF TABLES	vi
NOMENCLATURE	vii
Abstract	1
1. INTRODUCTION	2
2. EXPERIMENTAL PROCEDURE	4
2.1 Actual Mass Flow Rates Through Room Openings	6
2.2 Idealized Mass Flows Through Room Openings	7
3. ORIFICE COEFFICIENT THEORY	11
4. RESULTS AND DISCUSSION	18
5. CONCLUSIONS	24
6. ACKNOWLEDGMENTS	25
7. REFERENCES	25

LIST OF FIGURES

		Page
Figure 1.	Test room	31
Figure 2.	Gas burner locations	32
Figure 3.	Room opening configurations	33
Figure 4.	Two-layer approximation of opening temperature profile	34
Figure 5.	Transformations showing mappings from physical plane, to hodograph plane, to η plane, to t plane	35
Figure 6.	Transformation showing mapping of plan view of enclosure from physical plane to hodograph plane	36
Figure 7.	Vertical temperature profiles at different horizontal locations within doorway; H_o = 1.829 m, W_o = 0.737 m, $\dot{Q}$ = 63 kW	37
Figure 8.	Vertical velocity profiles at different horizontal locations within doorway; H_o = 1.829 m, W_o = 0.737 m, $\dot{Q}$ = 63 kW	38
Figure 9.	Horizontal velocity profiles at different vertical locations within doorway; H_o = 1.829 m, W_o = 0.737 m, $\dot{Q}$ = 63 kW	39
Figure 10.	Vertical temperature profiles measured by aspirated thermocouples in test room; H_o = 1.829 m, $\dot{Q}$ = 63 kW	40
Figure 11.	Mass flow rate vs. door width for fixed fire strength and door height	41
Figure 12.	Flow coefficients by Method A for a fixed door (0.74 x 1.83 m high) as a function of fire strength	42
Figure 13.	Outflow coefficients by Method B for a fixed doorway (0.74 x 1.83 m high) as a function of fire strength	43
Figure 14.	Flow coefficients by Method A for $\dot{Q}$ = 63 kW as a function of door width, H_o = 1.83 m	44
Figure 15.	Flow coefficients by Method B for $\dot{Q}$ = 63 kW as a function of door width, H_o = 1.83 m	45
Figure 16.	Flow coefficients by Method A as a function of window size for $\dot{Q}$ = 63 kW and W_o = 0.73 m	46
Figure 17.	Outflow coefficients by Method B as a function of window size for $\dot{Q}$ = 63 kW and W_o = 0.73 m	47

Figure 18. Theoretical orifice coefficient C plotted as function of opening to room width ratio b/h 48

Figure 19. Mass outflow rates predicted from temperatures 49

Figure 20. Mass inflow rates predicted from temperatures 50

LIST OF TABLES

Page

Table 1. Summary of experimental results 27

NOMENCLATURE

b	opening half width
C_i	inflow coefficient
C	theoretical orifice coefficient
C_o	outflow coefficient
g	gravitational acceleration
h	room or corridor half width
H_o	height of opening
ℓ	length of line burner
$\dot{m}_a$	average of actual mass inflow and outflow rates
$\dot{m}_{ia}$	mass inflow rate; actual
$\dot{m}_{ii}$	mass inflow rate; ideal
$\dot{m}_{oa}$	mass outflow rate; actual
$\dot{m}_{oi}$	mass outflow rate; ideal
N	height of neutral plane in the opening, $Z_n - Z_s$
Q	theoretical volume flux through orifice
$\dot{Q}$	fire strength
t	complex variable defined in eq. (15)
T	temperature within test room
T_a	ambient or reference temperature
$T_{g\ell}$	temperature of lower gas layer
T_{gu}	temperature of upper gas layer
$T_o(z)$	average temperature within opening at height Z
T_{or}	temperature within outer room
U	approach flow speed
U_∞	exit speed from orifice
v	magnitude of local velocity normal to opening

v_i	magnitude of velocity in opening jet
W	complex potential function $W = \phi + i\psi$
W_o	width of opening
x	coordinate in stream direction
y	coordinate across enclosure, corridor or opening
z	height above floor
Z	complex variable $x + iy$
Z_d	height above floor of interface between upper and lower gas layers in room
Z_n	height above floor of neutral plane in opening
Z_o	height of soffit above floor
Z_s	height of sill above floor
$\Delta p(z)$	static pressure difference across opening at height Z
ρ	local gas density within opening
ρ_a	density of air at temperature T_a
$\rho_o(z)$	average density within opening at height Z
ζ	complex hodograph variable $\zeta = u - iv$
η	auxiliary complex variable

FIRE INDUCED FLOWS THROUGH ROOM OPENINGS - FLOW COEFFICIENTS

K.D. Steckler, H.R. Baum and J.G. Quintiere

Abstract

A full-scale experimental and theoretical study was made of steady-state fire-induced flows through doorway and window openings. Measurements included two-dimensional temperature and pressure-difference profiles within the opening and vertical temperature profiles within the rooms connected by the openings. A floor-level gas burner served as the energy source. Mass flow rates through the openings were calculated from the opening data. A static-pressure flow model was used to establish ideal orifice flows from different combinations of the experimental temperature profiles. The opening and ideal flow results were combined to form room-opening flow coefficients as a function of fire energy release rate, opening geometry, and fire location. Two calculation procedures were used to compute the ideal flow. An irrotational jet model for the flow coefficients was developed and found to be in reasonable agreement with these and other measurements. Measured flow coefficient results show no significant dependence on fire strength, opening geometry, or fire location, as long as the ideal mass flow rate was based on measured gas temperatures. However, the theory indicates a significant variation in flow coefficient with opening widths larger than those used in the experiments.

1. INTRODUCTION

The flow of gas through openings in a room containing a fire represents a key element in the fire-growth process. Therefore, it is important to describe these flows correctly in mathematical models which simulate fire-growth in enclosures. In the zone modeling approach to fire growth [e.g., 1-4], which represents phenomena in discrete physical zones, these flows are computed based on conditions surrounding the opening. This computation requires knowledge of room-opening flow coefficients.

Early work in the mathematical prediction of room fires, done by Kawagoe [5] and Sekine [6], dealt with a fully-developed fire situation which was approximated as uniform in temperature. They treated the buoyancy-driven gas flow through the doorway or window opening as an orifice flow problem. A flow coefficient of 0.7 — taken from pipe-flow technology -- was assumed valid for these room openings. Thomas, Heselden, and Law [7] examined the problem of flow through both small and large openings in an enclosure containing a fully-developed fire. The small-opening flow was modeled as an orifice problem, whereas the large-opening flow was treated as an entrainment problem.

The orifice concept was carried over to zone models for the developing fire by Thomas, et al [8] who developed a two-layer model for gas flow through a roof vent, and Emmons [9], Rockett [10], and Zukoski [11], who modeled the doorway and window-opening versions of the problem. Here again, flow coefficients taken from pipe-flow technology were employed.

Prahl and Emmons [12] studied flows through a single window and single door opening with a reduced-scale kerosene/water analog experiment. Inflow and outflow orifice coefficients were determined and found to be significantly different at low Reynolds number (Re based on flow height), but tended to a common value of approximately 0.68 as the Reynolds number increased. In particular, they state that the outflow coefficient can be regarded as approximately 0.77 for $1000 < Re < 15{,}000$; although their results at high R_e tend to be lower than 0.77. The inflow coefficient was lower, but appeared to approach a value of 0.68 for $Re > 4000$ for the window and $Re > 10{,}000$ for the door configuration. For most full-scale fire conditions ($Re > 5000$ in the present study), the large Reynolds number case should apply. Then their results suggest the use of a constant coefficient value for both of approximately 0.68. The question remained, however, whether this flow coefficient, which was obtained for two different constant density liquid layers, was applicable to the flow of a variable density gas in a full-scale room geometry and for various opening configurations.

In the case of gas flows, Shaw [13] studied full-scale natural convection through rectangular openings in walls for space heating and ventilation applications. However, the temperature differentials in his work were limited to $12^{o}C$. His results show a flow coefficient of $0.65 \pm .05$ between temperature differentials of 4 to $10^{o}C$ with higher values outside this temperature range.

The present study describes full-scale experiments to measure fire-induced flows through room openings, and a theory for the attendant flow coefficients. The experiments represent conditions of developing room fires, before full involvement, and temperature differentials for the room gases

ranging from approximately 60 to 270°C. The effects on the coefficients of opening geometry, fire strength, fire location and ideal-flow model selected are examined. A discussion of the results of mass flow rate through the opening and on fire plume entrainment characteristics has been reported elsewhere [14].

2. EXPERIMENTAL PROCEDURE

Steady-state experiments were conducted in the 2.8 x 2.8 x 2.13 m test room shown in figure 1. The ceiling and walls were covered with a ceramic fiber insulation board to allow the room to reach quasi-steady test conditions in approximately 0.5 hr. A door or window opening was located on one wall. The vertical centerline of the opening either coincided with the centerline of the wall or was located 6.25 cm to one side.

The test room was located in a small room of a one-story building. This "outer-room" was maintained at nearly atmospheric conditions through the use of two roof vents, several windows, and one door opening. No experiments were conducted for external wind conditions in excess of 5 m/s.

A 0.305 m diameter floor-level diffusion gas burner served as the fire source. Commercial grade methane was supplied at a low momentum rate typical of natural fire pyrolysis rates. The burner was positioned in primarily three locations: the center of the room, the back left corner and the center of the rear wall relative to the wall with the opening. Other locations, with the burner face raised 0.3 m above the floor, were also examined. These configurations are illustrated in figure 2.

Movable bidirectional probes [15] with attached bare-wire thermocouples were used to determine gas velocities and temperatures at points on a two-dimensional grid which spanned the entire area of the room opening. The axes of the bidirectional probe sensing heads were aligned normal to the opening. The measurement plane was located at the mid-plane of the 102 mm deep jamb. The horizontal spacing between grid points varied between 65.1 and 111 mm depending on the width of the opening. With one exception the vertical spacing was fixed at 114 mm. The exception was the smallest window in which the spacing was reduced to 51 mm. These spacings produced between 64 and 144 measurement points depending on the area of the opening. The door and window configurations selected for study are shown in figure 3.

Vertical gas temperature profiles were measured on both sides of the room wall containing the opening. Aspirated thermocouples similar to those of Newman and Croce [16] were used in the test room while bare-wire thermocouples were used in the outer room. In both cases, vertical spacing between thermocouples was 114 mm.

All thermocouple junctions used in this study were formed by welding the overlapping ends of 0.254 mm chromel and 0.254 mm alumel wires. No radiation corrections were applied to the thermocouple data. Nevertheless, estimates of the radiation error were used in assigning error bands to the flow coefficient results.

Experiments were designed to determine the effect of room-opening geometry, fire strength, and fire location on the opening flows and flow coefficients. Fire strength, $\dot{Q}$, is defined as the product of the fuel flow

rate and lower heating value of the fuel. The fire strength ranged from 31.6 to 158 kW.

Inflow and outflow coefficients, C_i and C_o, were computed as the ratios of experimental to idealized mass flow rates (see eqs. (10) and (11) below. In this context, "idealized flows" are derived using Bernoulli's equation and principles of hydrosatics. Two expressions will be examined for the idealized mass flow rates.

2.1 Actual Mass Flow Rates Through Room Openings

Experimental or "actual" mass flow rates and velocities were calculated from the opening temperature and bidirectional probe data. Actual mass flow rates were obtained by integrating the local mass velocities, ρv, over the flow area. The local density ρ was obtained from the measured local temperature and the ideal gas law. Actual flow into the room, $\dot{m}_{ia}$, occurs over the opening width, W_o, and over the height between the sill, Z_s, and neutral plane or zero-velocity point within the opening, Z_n. Actual flow from the room, $\dot{m}_{oa}$, occurs over the height between Z_n and the soffit, Z_o. Therefore

$$\dot{m}_{ia} = \int_0^{W_o} \int_{Z_s}^{Z_n} \rho v \, dz \, dy \qquad (1)$$

and

$$\dot{m}_{oa} = \int_0^{W_o} \int_{Z_n}^{Z_o} \rho v \, dz \, dy \qquad (2)$$

These integrations were carried out numerically using the trapazodial rule in the vertical direction and the rectangular rule in the horizontal direction. The gas velocities at the surface interface were taken as zero.

2.2 Idealized Mass Flows Through Room Openings

A static pressure ideal gas flow model was used to establish the idealized opening flows in terms of the room and/or opening experimental temperature profiles. Two methods of calculation were employed. The first, designated Method A, follows the analysis of Quintiere and DenBraven [17]. This method uses the ideal gas law to express the differences between the static pressure profiles in the rooms connected by the opening, $\Delta p(z)$, in terms of the vertical temperature profiles measured in these rooms; $T(z)$ in the test room and $T_{or}(z)$ in the outer room. Variables at the opening are considered to depend only on z. Hence horizontally averaged temperatures in the opening, $T_o(z)$, will be used in computing the idealized flow. The opening gas density, $\rho_o(z)$, is accordingly computed from $T_o(z)$ since ρT is a constant. The idealized velocity profile at the opening, $v_i(z)$, is obtained by applying Bernoulli's equation along assumed horizontal streamlines which start from rest at points "far" from the opening and terminate at the opening where

$$v_i(z) = \sqrt{2\Delta p(z)/\rho_o(z)} \qquad (3)$$

The static pressure difference $\Delta p(z)$ is computed from the temperature distributions on either side of the opening, $T(z)$ and $T_{or}(z)$, and the neutral plane height, Z_n . One temperature, or pressure, distribution refers to the fluid in the rest state, the other distribution refers to the fluid surrounding the

jet as it enters or leaves the room through the opening. For concurrent flow in a simple orifice, the latter pressure distribution strictly applies just downstream of the orifice at the vena contracta of the jet. The flow coefficient, to a large extent, then reflects the difference between the flow area at the orifice opening and the flow area at the vena contracta. In computing the idealized flow for the countercurrent case, the flow area at the opening is used. The mass velocity, $\rho_o v_i$, is then formed and integrated over the area of flow within the opening to produce the ideal mass outflow rate

$$\dot{m}_{oi} = W_o \rho_a T_a \sqrt{2g} \int_{Z_n}^{Z_o} \sqrt{\frac{1}{T_o} \int_{Z_n}^{z} \left(\frac{1}{T_{or}} - \frac{1}{T}\right) dz'} \, dz \qquad (4)$$

and ideal mass inflow rate

$$\dot{m}_{ii} = W_o \rho_a T_a \sqrt{2g} \int_{Z_s}^{Z_n} \sqrt{\frac{1}{T_o} \int_{z}^{Z_n} \left(\frac{1}{T_{or}} - \frac{1}{T}\right) dz'} \, dz \qquad (5)$$

The fact that the velocity profile at the opening differs from v_i, or alternatively, that the area of flow at the vena contracta differs from the flow area within the opening is accounted for in the flow coefficient.

The second calculation method was based on a two-layer temperature profile as defined by Emmons [18]. This is designated as Method B. The motivation for this approach was to provide some compatiblity between the flow coefficient and its use in zone modeling wherein the room gas temperature distribution is represented as constant in the upper and lower regions. This method requires an interpretation of the experimental data into a two-step profile. The idealized outflow, defined by this two-layer temperature profile is

$$\dot{m}_{oi} = \frac{2}{3} W_o \rho_a T_a \sqrt{2g} \sqrt{\frac{1}{T_{gu}} \left(\frac{1}{T_a} - \frac{1}{T_{gu}}\right)} \, (Z_o - Z_n)^{3/2} \qquad (6)$$

where T_{gu} represents the temperature of a uniform upper gas layer within the room and T_a represents the temperature of a uniform single gas layer located outside the room. Equation (6) follows directly from eq. (4) for this two-step temperature profile.

Effective values for T_{gu}, T_a, and Z_n are obtained from the experimental data taken within the opening by constructing a two-layer approximation to the opening temperature profile as depicted in figure 4. First T_a is set equal to the average of the temperatures measured in the lower opening. Then T_{gu} and Z_n are established subject to the physical condition that the experimental and idealized opening temperature profiles represent equal masses of gas per unit horizontal area,

$$\int_{Z_s}^{Z_o} \frac{1}{T_o(Z)}\, dz = (Z_n - Z_s)/T_a + (Z_o - Z_n)/T_{gu}, \qquad (7)$$

and the arbitrary condition that the temperature integrals are equal such that

$$\int_{Z_s}^{Z_o} T_o(z)\, dz = (Z_n - Z_s)\, T_a + (Z_o - Z_n)\, T_{gu}\ . \qquad (8)$$

The integrations in equations (4), (5), (7), and (8) were carried out numerically.

A corresponding ideal inflow mass flow rate can also be defined in terms of a two-layer temperature model. It becomes more difficult, however, to convert the experimental profiles into equivalent two-step temperature profiles. For a room temperature represented by a step profile (T_a, T_{gu}), the ideal inflow rate follows from eq. (5) as follows:

$$\frac{2}{3} W_o \rho_a T_a \sqrt{2g} \sqrt{\frac{1}{T_a}\left(\frac{1}{T_a} - \frac{1}{T_{gu}}\right)}$$

$$\dot{m}_{ii} = \begin{cases} \cdot (Z_n - Z_d)^{1/2} \left(Z_n + \frac{Z_d}{2} - \frac{3}{2} Z_s\right) ; \text{ when } Z_d \geq Z_s & (9a) \\ \\ \frac{2}{3} W_o \rho_a T_a \sqrt{2g} \sqrt{\frac{1}{T_a}\left(\frac{1}{T_a} - \frac{1}{T_{gu}}\right)} \\ \\ \cdot (Z_n - Z_s)^{3/2}; \text{ when } Z_d \leq Z_s & (9b) \end{cases}$$

where Z_d is the height of the interface between the upper and lower layers within the room. In this case, the corresponding two-step profile can be determined from the room temperature data and equations (7) and (8). The inability of this procedure to provide a good approximation to the temperature data and its impact on the flow coefficient will be discussed later.

For both methods, the flow coefficients are defined as

$$C_o = \dot{m}_{oa}/\dot{m}_{oi} \tag{10}$$

for outflow, and

$$C_i = \dot{m}_{ia}/\dot{m}_{ii} \tag{11}$$

for inflow.

For both Method A and Method B, the extent to which the assumptions used to develop the ideal flows deviate from reality will be reflected in differences between the ideal and actual flows; namely, the flow coefficients.

3. ORIFICE COEFFICIENT THEORY

The use of orifice models to predict room opening mass flows in zone models suggests that the underlying physics might be used to calculate the orifice coefficient itself. The flow in the doorway or window is assumed to be dominated by the horizontal contraction and acceleration induced by the hydrostatic pressure drop at a given height across the opening. The effects of variable density, three dimensionality, turbulence, viscosity, and thermal conductivity on the motion are omitted. The problem then reduces to the calculation of a two dimensional irrotational jet. The jet is generated when a uniform approach flow of speed U in a room or corridor of half width h is accelerated through an opening of half width $b < h$ (see figure 5a). The uniform flow originates either outside the room or corridor, or in the buoyant plume generated by the enclosure fire. In the latter case, the conditions under which the uniform flow assumption is reasonable are examined by a separate analysis.

The flow can be described in terms of a complex potential function W(Z), defined by the following relations:

$$W(Z) \equiv \phi(x,y) + i\psi(x,y)$$

$$\frac{dW}{dZ} \equiv \zeta = u(x,y) - iv(x,y) \qquad (12)$$

$$Z = x + iy$$

Here ϕ is the velocity potential, ψ is the stream function, while u and v are the velocity components in the x and y coordinate directions respectively. The boundary conditions are:

$$\zeta(-\infty) = U$$

$$\psi(x,o) = 0$$

$$\psi = Uh \text{ along ABCD} \qquad (13)$$

$$u^2 + v^2 = U_\infty^2 \text{ along CD}$$

Note that neither the location of the curve CD nor the limiting downstream speed U_∞ are known a priori. Once they are determined as part of the solution, then the orifice coefficient C is given by:

$$C = \frac{Uh}{U_\infty b} \qquad (14)$$

The solution procedure rests on the fact that the flow boundaries have a very simple shape in the ζ (hodograph) plane (figure 5b). The velocity on streamline $\psi = Uh$ decreases horizontally along the wall from A to B. The corner B at $Z = ih$ is a stagnation point $\zeta = 0$. The velocity on this streamline then increases along the wall in the negative y direction until the unknown speed U_∞ is reached at the opening point C, where $Z = ib$. The streamline then turns at constant speed until the direction parallel to the x-axis is reached at D. Thus, in the ζ plane, the curve CD is the arc of a circle of radius U_∞. The velocity on the streamline $\psi = 0$ increases

horizontally from A to D, as the flow is accelerated from velocity U at $x = -\infty$ to U_∞ at $x = +\infty$. The restriction to a symmetrical geometry is not essential, but it greatly simplifies the algebra with little loss in basic understanding or ability to compare theory and experiment.

The use of the hodograph plane to solve problems of this type dates back over a century to Kirchhoff, who solved this problem in the limit $h \to \infty$. This and subsequent developments are described in Lamb [23]. The sequence of conformal mappings and "solution by inspection" needed for the present problem are as follows:

i) $\eta = \zeta^2$

This maps the domain in the ζ plane into a semicircle of radius U_∞^2 in the η plane (figure 5c).

ii) $t = -(\eta + U_\infty^4/\eta)$

This maps the domain in the η plane into the upper half t-plane (figure 5d).

iii) The complex potential W(t) must vanish at infinity and satisfy the following conditions on the real axis in the t plane.

$$\text{Im}\{W(t)\} = Uh;\ \text{Re}(t) > -2\,U_\infty^2$$

$$\text{Im}\{W(t)\} = 0;\ -\left(U^2 + U_\infty^4/U^2\right) < \text{Re}(t) < -2U_\infty^2$$

$$\text{Im}\{W(t)\} = Uh;\ \text{Re}(t) < -\left(U^2 + U_\infty^4/U^2\right)$$

The unique non-singular function satisfying these conditions is:

$$W(t) = \frac{Uh}{\pi}\left\{\log\left[t + \left(U^2 + U_\infty^4/U^2\right)\right] - \log\left[t + 2U_\infty^2\right] + i\pi\right\}$$

$$t = -\left(\zeta^2 + U_\infty^4/\zeta^2\right). \qquad (15)$$

The physical coordinate can be recovered by noting that the point Z = ih is a stagnation point (see figure 5a). Thus

$$Z = ih + \int_0^\zeta \frac{dW}{d\zeta}\frac{d\zeta}{\zeta} \qquad (16)$$

Inserting eq. (15) in eq. (16), the solution can be written in dimensionless form as

$$\frac{Z}{h} = i + \frac{4}{\pi}(U/U_\infty)\left\{\frac{1}{2}\log\left[(1+\bar{\zeta})/(1-\bar{\zeta})\right]\right.$$

$$-\frac{1}{4}(U_\infty/U)\log\left[(1+U_\infty\bar{\zeta}/U)/(1-U_\infty\bar{\zeta}/U)\right]$$

$$\left.-\frac{1}{4}(U/U_\infty)\log\left[(1+U\bar{\zeta}/U_\infty)/(1-U\bar{\zeta}/U_\infty)\right]\right\} \qquad (17)$$

$$\frac{W}{Uh} = \frac{1}{\pi}\left\{\log\left[(U/U_\infty)^2 + (U_\infty/U)^2 - (\bar{\zeta}^2 + 1/\bar{\zeta}^2)\right]\right.$$

$$\left.-\log\left[2 - (\bar{\zeta}^2 + 1/\bar{\zeta}^2)\right] + i\pi\right\}$$

$$\bar{\zeta} = (u - iv)/U_\infty$$

The final step in the analysis is the calculation of the ratio U/U_∞, which determines the orifice coefficient (see eq. 14). This is done by enforcing the condition (see figure 5a)

$$Z = ib \quad @ \quad \zeta = iU_\infty. \qquad (18)$$

This is most conveniently done using eqs. (15) and (16) directly and noting that ζ is imaginary along the integration path. The result is

$$\frac{b}{h} = 1 + \frac{4}{\pi}(U/U_\infty)\left\{\frac{\pi}{4} - \frac{1}{2}(U_\infty/U)\tan^{-1}(U_\infty/U)\right.$$

$$\left.-\frac{1}{2}(U/U_\infty)\tan^{-1}(U/U_\infty)\right\} \qquad (19)$$

Eqs. (14) and (19) together are a formula for the orifice coefficient C as a function of b/h, expressed parametrically in terms of the velocity ratio U/U_∞ The two limiting cases provide ready checks on the analysis. When b/h = 1, the problem degenerates to a uniform flow in a channel, i.e.:

$$b/h = U/U_\infty = C = 1$$

When $b/h \to 0$, with $Uh \equiv Q$ fixed, then the classical Kirchhoff result [23] is recovered.

$$b = (Q/U_\infty)\ (1 + 2/\pi)$$

$$C = \pi/(\pi + 2)$$

Finally, some assessment of the conditions under which the approach flow in horizontal planes might be reasonably uniform for the case of an outflow can be made. Let the outflow from the fire plume at a given height be represented by a point source of strength 2Uh located at the point x_o, y_o in the enclosure (figure 6a). The flow is assumed to be a plane potential flow. While this is certainly unrealistic, all the neglected effects will tend to make the actual flow uniform more quickly than in this calculation. Hence, the distance between the fire plume and the opening needed for the approach flow to be considered uniform can be estimated from this calculation with confidence that the estimate is conservative.

The solution is obtained by noting that the transformation defined by

$$\zeta \equiv \xi + i\eta = \sinh\left(\frac{\pi Z}{2h}\right)$$

$$Z \equiv x + iy \tag{20}$$

maps the interior of the enclosure in the Z plane into the right half ζ plane (figure 6b). The complex potential then is the sum of the original source plus its image at $(-\xi_o, \eta_o)$

$$W(\zeta) \equiv \phi + i\psi = \frac{Uh}{\pi}\left\{\log(\zeta-\zeta_o) + \log(\zeta+\bar{\zeta}_o)\right\}$$

$$\xi = \sinh\left(\frac{\pi x}{2h}\right)\cos\left(\frac{\pi y}{2h}\right)$$

$$\eta = \cosh\left(\frac{\pi x}{2h}\right)\sin\left(\frac{\pi y}{2h}\right) \tag{21}$$

$$\zeta_o \equiv \rho(x_o, y_o) \equiv \xi_o + i\eta_o$$

$$\bar{\zeta}_o \equiv \xi_o - i\eta_o$$

Now suppose that $x-x_o > 2h$; i.e. the point under consideration is at least one room width away from the center of the plume. Then, the complex velocity field dW/dZ can be approximated to better than one percent by:

$$u - iv \tilde{=} \frac{U}{2}\left\{(1-\zeta_o/\zeta)^{-1} + (1+\bar{\zeta}_o/\zeta)^{-1}\right\} \tag{22}$$

However, under these circumstances

$$\left|\frac{\bar{\zeta}_o}{\zeta}\right| < \left|\frac{\zeta_o}{\zeta}\right| < e^{-\pi} \tilde{=} .043$$

Thus, if the door opening is more than one room (or corridor) width from the fire plume, the approach velocity should be reasonably uniform in a horizontal plane. The effects of vertical mixing and density variations of all kinds remain unaccounted for, however.

4. RESULTS AND DISCUSSION

Before considering the results for the flow coefficients, some characteristics of the temperature and flow fields will be examined. The room corner and center fires will be used for illustration since those results tend to bracket the data for all the conditions. Detailed listings of the temperatures, velocities, and mass flows for all experiments conducted in this study can be found in ref. [19]. Representative vertical temperature profiles within a room opening for both center and corner 63 kW fires are displayed in figure 7. These typical data show a shift from a fairly well defined two-layer flow to a much more stratified flow as the burner is moved from the center to corner position. The Z_n values shown in these and subsequent figures represent the experimental zero-velocity heights within the openings.

Attendant velocity profiles presented in figures 8 and 9 show that the opening flow velocities are lower for the corner fire than for the center fire. Throughout this study, for a given opening geometry and fire strength, the opening velocities were lower for the corner fire.

Many of the horizontal velocity profiles mapped in this study exhibit centerline velocities which are low relative to velocities closer to the jamb for the same height. The result is the "dished" appearance shown in most of

figure 9a and to a lesser extent in figure 9b. This concave appearance of the profiles has an explanation offered by potential flow theory [20], and is a result of the theory presented herein; however, other variations must be attributed to the velocity probe or non-uniform ambient conditions.

Figure 10 shows typical test room temperature profiles for both center and corner 63 kW fires as a function of door width. In contrast to the doorway temperature profiles of figure 7, these profiles show a uniform temperature in the upper and lower regions more consistent with the idealized profiles of the two-layer zone models. Although upper and lower layers might be defined by these uniform temperature regions, the transition between them is not sharp and the lower layer temperature is greater than the inlet air temperature. For either fire location, the temperature and depth of the upper layer increases as the door width decreases. However, for a given opening geometry and fire strength, the corner fire produces a hotter and thinner upper layer. These variations are similar to those reported by McCaffrey and Rockett [21], and may be a general effect of fire location.

Doorway neutral plane heights, Z_n, are also displayed in figure 10. Note that for the center burner configuration (figure 10a) Z_n is either within or above the transition zone or "interface" between the upper and lower layer. However, for the corner fire configurations (figure 10b) Z_n is below the interface. The position of Z_n relative to the interface is important when one attempts to compute the idealized mass inflow rate for Method B. Also it has been shown [21] that the actual temperature in the lower layer, necessarily greater than the inlet air, must be used to predict more accurately the pressure difference across the room opening. Since this pressure difference

controls the flow rate, it is easy to see why an overly constrained step-profile for Method B can lead to poor results.

Examples of actual mass flow rates are illustrated in figure 11 as a function of width for the door configuration. Inflow and outflow rates for a given test fall within ± 3.1% of the average of these two values. Indeed, with the exception of the smallest window, all configurations examined in this study yielded deviations between inflow and outflow within this range. The deviation is ± 7% for the smallest window. In general, the mass flow rates are smallest for the corner fire location because the fire plume entrains less gas in this position [14]. It is significant to note that the mass flow rate in figure 11 is not directly proportional to W_o nor $W_o H_o^{3/2}$ as is frequently assumed.

In addition to these experiments, more recent results have been added for a line-burner fire, positioned at the rear wall on the floor (see figure 2). A summary of results for all the experimental conditions are listed in table 1 (4 pages). The zero-velocity neutral plane position, relative to the bottom of the opening, $N = Z_n - Z_s$, is fairly constant at approximately half of the opening height. This position was determined from the velocity data. In contrast, the thermal interface between the upper and lower layers in the room varies significantly. This height, Z_d, was estimated at the mid point of the transition region between the approximate uniform upper and lower temperature regions. The extent of the transition zone is also noted, and the average

values of the experimental upper and lower temperatures are tabulated.* Thus, approximate temperature profiles could be constructed from these data in a form similar to those of figure 10. Finally, the flow coefficients are listed for Methods A and B. Only the outflow coefficient is shown for Method B because the results for the inflow coefficient showed a significant dependence on door width and this computation was not pursued further [22]. The inflow coefficient decreased nearly linearly from 0.62 to 0.48 from the smallest to largest door width. Moreover, the two-step temperature profile used in Method B was a poor approximation to the measured room temperatures.

The results for the flow coefficients will now be examined in more detail. Also, in the following figures, "error bars" are included which represent the maximum uncertainty in the results. These uncertainties were determined by estimating errors in the velocity and temperature measurements and then computing the maximum deviations of the flow rates and coefficients about their measured values [19]. The most significant uncertainty is due to estimates of radiation error in the temperature measurements at near ambient temperature; however, the error estimate is most conservative in that temperature range. The flow coefficients were computed by eqs. (10) and (11) using the average value of the measured in and outflows. Hence, some uncertainty in the coefficients results from descrepancies between these flow measurements.

Figures 12 and 13 display the flow coefficients computed by both methods as a function of the fire size. This is shown for three burner locations - center, wall and corner - for a fixed door opening - 0.74 x 1.83 m high.

*Note that these temperatures are arithmetic averages of the experimental data and <u>not</u> effective values computed by eqs. (7) and (8).

Method A yields essentially constant values: 0.70-0.75 for C_o and 0.65-0.73 for C_i. The large uncertainty in C_i at small fires is due to the conservative estimate of radiation error on the thermocouples which in turn causes significant variations in the ideal mass flow rate. Indeed, this reflects the sensitivity of the ideal flows to the temperature profile and contributes to the wider variation of results by Method B: $0.76 \leq C_o \leq 1.0$ as shown in figure 13.

Similar results are shown in figures 14-17 when the effect of door and window size are examined for a fixed fire strength, $\dot{Q}$ = 63 kW. The flow coefficients by Method A appear to remain fairly constant, independent of fire location and opening size, with the outflow values slightly higher than the inflow coefficients. Considerably more variation is shown for Method B.

The calculated orifice coefficient is plotted as a function of b/h in figure 18. The experimentally determined coefficients are also replotted here in terms of the b/h ratio appropriate to the room of origin of the flow. To permit the most appropriate comparison between experiment and theory, only coefficients from experiments involving symmetric geometries consistent with the uniform-flow assumption are displayed. The slow upward trend predicted by potential flow theory is clearly observeable, although the calculated results are about 15 percent low. This result is highly encouraging, considering the simplicity of the approach. Further support for the theory comes from the shape of the profiles in figure 9. It is well known [20] that in a potential flow the speed is greatest at a flow boundary. This requirement, together with the assumption of flow symmetry with respect to the doorway centerline leads to the dish shaped speed profiles seen in figure 9.

In order to gain insight into the sources of the discrepancy shown in figure 18, it is useful to examine the experiments of Prahl and Emmons [12]. Their experiments were performed with opposed uniform kerosene and water streams, eliminating both variable density and non-uniform flow effects. The reported orifice coefficients are strongly dependent on Reynolds number, due to the small scale of the experiments. If one restricts attention to the data corresponding to Reynolds numbers above 10^4, as displayed in figure 9 of ref. [12], the doorway coefficients converge asymptotically within a band between 0.6 and 0.7, with an average value of about 0.65. Since the corresponding theoretical value for this configuration is 0.62, the non-uniformity of the approach flow and density variations in each stream seem to be the principal sources of error.

Finally all of the circular burner results for the center, wall, corner and elevated locations are displayed in figures 19 and 20 where the measured mass flow rates are plotted against the idealized mass flow rates by Method A for the outflow and inflow respectively. These results follow a linear dependence with the slope representing a nominal flow coefficient. A linear fit to the data yields an average outflow coefficient of 0.73 and an average inflow coefficient of 0.68. Additional results, presented in table 1 for the line burner at the rear wall, show flow coefficients consistent with these average values. Moreover Method A gives results that differ little from these mean values.

5. CONCLUSIONS

For the range of conditions in this study, the flow coefficients derived by Method A are fairly invariant with fire size, location and opening configuration. The mean value of the inflow coefficient is 0.68 and 0.73 for the outflow coefficient. The variation of the data about these mean values is less than ± 0.05. Although the uncertainty in the results is greater than this deviation in some instances, this is due to the sensitivity of the error analysis on thermocouple corrections at low temperatures.

The measured coefficients agree reasonably well with predictions based on two dimensional potential flow. The most important discrepancies between theory and experiment appear to be due to density variations in three dimensions. The theory predicts a systematic variation of orifice coefficient with ratio of vent width to room of origin width. However, this variation is small in the parameter range investigated in most fire experiments to date.

Within the range of the opening configurations and fires studied the derived flow coefficients could be used together with the idealized equations given here to calculate door or window flows in fire experiments. Hence temperature data, without the expenditure of numerous velocity probes, are sufficient to calculate the flow. This technique could be of significant value in fire experiments.

The results for flow coefficients also provide improved data for use in the current zone models to predict room fire growth [1-4]. Although a question of consistency between Methods A and B and a two-layer room fire model

remains, the results presented provide improved insight on the variations of C_i and C_o under realistic fire conditions. As long as the predictions of temperature from models are in good agreement with the data, then the flow calculations for the flow coefficients of Method A will give accurate results.

6. ACKNOWLEDGMENTS

We are grateful to Armstrong World Industries for their partial support of this project through the National Bureau of Standards Research Associate Program. We are indebted to William Rinkinen and cooperative-education interns Cho Sze, Wendy Wussow, Adalberto Maldonado and Michael Beaupre for their assistance with the experiments and data reduction.

7. REFERENCES

1. Quintiere, J.G., Growth of Fire in Building Compartments, Fire Standards and Safety, ASTM STP 614, 1977, p. 131.

2. Emmons, H.W., Mitler, H.E. and Trefethen, L.N., Computer Fire Code III, Home Fire Project Technical Report No. 25, Harvard Univeristy, 1978.

3. Pape, R. and Waterman, T., Modification to the RFIRES Preflashover Room Fire Computer Model, IITRI Project J6400, IIT Research Institute, Chicago, IL, March 1977.

4. MacArthur, C.D. and Myers, J.F., Dayton Aircraft Cabin Fire Model Validation, Phase I, Report No. FAA-RD-78-57, University of Dayton Research Institute, Dayton, OH, March 1978.

5. Kawagoe, K., Fire Behavior in Rooms, Report No. 27, The Building Research Institute, Japan, Sept. 1958.

6. Sekine, T., Room Temperature in Fire of a Fire-Resistive Room, Report No. 29, The Building Research Institute, Japan, March 1959.

7. Thomas, P.H., Heselden, A.J.M. and Law, M., Fully-Developed Compartment Fires -- Two Kinds of Behavior, F.R. Technical Paper No. 18, Fire Research Station, Borehamwood, England, Oct. 1967.

8. Thomas, P.H., Hinkley, P.L., Theobald, C.R. and Simms, D.L., Investigations into the Flow of Hot Gases in Roof Venting, F.R. Technical Paper No. 7, Dept. of Scientific and Industrial Research and Fire Offices' Committee Joint Research Organization, London, 1963.

9. Emmons, H.W., Natural Convective Flow Through an Opening, Part I, Home Fire Project Technical Report No. 1, Harvard University, 1973.

10. Rockett, J.A., Combustion and Flame, 12:165-175 (1976).

11. Zukoski, E.E., Convective Flows Associated with Room Fires, Semi-Annual Progress Report, NSF GI 31892XI, California Institute of Technology, Pasadena, CA, June 1975.

12. Prahl, J. and Emmons, H.W., Combustion and Flame, 25:369-385 (1975).

13. Shaw, B.H., Heat and Mass Transfer by Combined Forced and Natural Convection, Institution of Mechanical Engineers Symposium, University of Manchester, Owens Park, England, Sept. 15, 1971, Paper C117/71, p. 31-39.

14. Steckler, K.D., 19th Symposium (Int.) on Combustion, The Combustion Institute, 1983.

15. McCaffrey, B.J. and Heskestad, G., Combustion and Flame, 26:125-127 (1976).

16. Newman, J.S. and Croce, P.A., Journal of Fire and Flammability, 10:326-336 (1979).

17. Quintiere, J.B. and DenBraven, K., Some Theoretical Aspects of Fire Induced Flows Through Doorways in a Room-Corridor Scale Model, NBSIR 78-1512, National Bureau of Standards, Washington, DC, Oct. 1978.

18. Emmons, H.W., Personal Communication, 1979.

19. Steckler, K.D., Quintiere, J.G. and Rinkinen, W.J., Flow Induced by Fire in a Compartment, NBSIR 82-2520, National Bureau of Standards, Washington, DC, Sept. 1982.

20. Batchelor, G.K., An Introduction to Fluid Dynamics, Cambridge University Press 1967, p. 384.

21. McCaffrey, B.J. and Rockett, J.A., Journal of Research of the National Bureau of Standards, 82:107-117 (1977).

22. Steckler, K.D., "Fire Induced Flows Through Room Openings", Tech. Res. Rep. Project 203005-003, Armstrong Cork Co., Research and Development, May 13, 1981.

23. Lamb, H., Hydrodynamics, Dover, NY, p. 94, 1945.

Table 1. Summary of Experimental Results

Opening Configuration (Fig. 3)	Fire Strength Q (kW)	Fire Location (Fig. 2)	Air Mass Flow Rate $\dot{m}_a$ (kg/s)	Neutral Plane Location N/H_o	Thermal Interface Height Z_d (m)	Avg. Temp. of Upper Gas Layer T_{gu} (°C)	Avg. Temp. of Lower Gas Layer T_{gl} (°C)	Ambient Temperature T_a (°C)	Method A C_o	Method A C_t	Method B C_o
2/6 Door	62.9	A	0.251	0.499	0.57 ± 0.28	190	72	26	0.73	0.69	0.74
3/6 Door	62.9	A	0.358	0.514	0.74 ± 0.23	164	62	28	0.73	0.71	0.76
4/6 Door	62.9	A	0.457	0.531	0.86 ± 0.23	141	50	22	0.74	0.72	0.77
4/6 Door	62.9	A	0.465	0.536	0.86 ± 0.23	135	39	13	0.74	0.70	0.76
5/6 Door	62.9	A	0.523	0.552	0.91 ± 0.17	129	47	23	0.74	0.67	0.78
6/6 Door	62.9	A	0.563	0.562	0.97 ± 0.23	129	48	29	0.72	0.66	0.80
6/6 Door	62.9	A	0.560	0.561	0.91 ± 0.17	130	51	31	0.72	0.66	0.81
6/6 Door	62.9	A	0.624	0.556	1.03 ± 0.17	109	33	12	0.75	0.71	0.80
6/6 Door	62.9	A	0.605	0.557	1.03 ± 0.17	116	34	13	0.72	0.70	0.80
7/6 Door	62.9	A	0.616	0.573	1.03 ± 0.17	120	44	26	0.72	0.68	0.80
8/6 Door	62.9	A	0.677	0.582	1.09 ± 0.23	109	36	22	0.72	0.68	0.84
Full Window	62.9	A	0.464	0.501	0.74 ± 0.34	143	53	30	0.74	0.71	0.75
2/3 Window	62.9	A	0.302	0.485	0.74 ± 0.34	177	78	26	0.78	0.71	0.76
2/3 Window	62.9	A	0.304	0.484	0.74 ± 0.34	177	79	26	0.78	0.72	0.79
1/3 Window	62.9	A	0.117	0.453	0.80 ± 0.17	270	157	16	0.71	0.70	0.74
6/6 Door	31.6	A	0.446	0.569	0.97 ± 0.11	86	41	29	0.70	0.66	0.78
6/6 Door	105.3	A	0.624	0.547	0.97 ± 0.11	183	69	35	0.72	0.67	0.79
6/6 Door	158.0	A	0.688	0.535	0.91 ± 0.17	243	81	36	0.72	0.68	0.80
2/6 Door	62.9	B	0.203	0.523	1.14 ± 0.17	248	74	32	0.70	0.70	0.75
3/6 Door	62.9	B	0.286	0.556	1.14 ± 0.17	216	59	30	0.76	0.70	0.85
4/6 Door	62.9	B	0.354	0.568	1.31 ± 0.12	194	48	24	0.76	0.69	0.93

Table 1 (continued)

Opening Configuration (Fig. 3)	Fire Strength Q (kW)	Fire Location (Fig. 2)	Air Mass Flow Rate $\dot{m}_a$ (kg/s)	Neutral Plane Location N/H_o	Thermal Interface Height Z_d (m)	Avg. Temp. of Upper Gas Layer T_{gu} (°C)	Avg. Temp. of Lower Gas Layer $T_{g\ell}$ (°C)	Ambient Temperature T_a (°C)	Method A C_o	Method A C_1	Method B C_o
5/6 door	62.9	B	0.380	0.566	1.31 ± 0.23	197	51	29	0.71	0.64	0.90
6/6 door	62.9	B	0.442	0.566	1.37 ± 0.17	181	38	21	0.72	0.69	0.95
6/6 door	62.9	B	0.439	0.568	1.37 ± 0.17	186	51	30	0.72	0.65	0.92
6/6 door	62.9	B	0.449	0.571	1.37 ± 0.17	176	36	20	0.75	0.70	1.01
7/6 door	62.9	B	0.474	0.564	1.43 ± 0.23	179	47	29	0.70	0.65	0.96
8/6 door	62.9	B	0.502	0.586	1.49 ± 0.17	172	44	29	0.73	0.63	1.01
Full window	62.9	B	0.355	0.552	1.37 ± 0.17	194	50	28	0.73	0.71	0.88
2/3 window	62.9	B	0.245	0.499	1.37 ± 0.17	216	65	26	0.65	0.72	0.74
2/3 window	62.9	B	0.257	0.511	1.37 ± 0.17	215	62	23	0.69	0.70	0.80
6/6 door	31.6	B	0.345	0.580	1.37 ± 0.17	118	37	26	0.70	0.67	0.94
6/6 door	105.3	B	0.502	0.546	1.31 ± 0.23	234	51	27	0.72	0.68	0.90
2/6 door	62.9	C	0.243	0.528	1.03 ± 0.17	209	53	9	0.73	0.72	0.76
3/6 door	62.9	C	0.340	0.560	1.09 ± 0.23	173	34	7	0.77	0.73	0.83
4/6 door	62.9	C	0.388	0.566	1.14 ± 0.17	173	46	21	0.74	0.70	0.82
5/6 door	62.9	C	0.441	0.577	1.20 ± 0.23	160	41	20	0.74	0.68	0.84
6/6 door	62.9	C	0.488	0.579	1.26 ± 0.17	152	36	18	0.72	0.69	0.88
6/6 door	62.9	C	0.475	0.572	1.26 ± 0.17	156	41	23	0.71	0.69	0.84
7/6 door	62.9	C	0.549	0.591	1.26 ± 0.17	140	29	14	0.76	0.68	0.97
8/6 door	62.9	C	0.584	0.593	1.31 ± 0.11	134	29	15	0.74	0.68	0.98

Table 1 (continued)

Opening Configuration (Fig. 3)	Fire Strength Q (kW)	Fire Location (Fig. 2)	Air Mass Flow Rate $\dot{m}_a$ (kg/s)	Neutral Plane Location N/H_o	Thermal Interface Height Z_d (m)	Avg. Temp. of Upper Gas Layer T_{gu} (°C)	Avg. Temp. of Lower Gas Layer T_{gl} (°C)	Ambient Temperature T_a (°C)	Method A C_o	Method A C_i	Method B C_o
Full Window	62.9	C	0.438	0.562	1.26 ± 0.17	153	32	10	0.77	0.70	0.85
Full Window	62.9	C	0.421	0.552	1.26 ± 0.17	158	35	14	0.74	0.72	0.81
2/3 Window	62.9	C	0.306	0.488	1.14 ± 0.17	178	48	9	0.73	0.70	0.78
1/3 Window	62.9	C	0.117	0.450	1.09 ± 0.23	288	153	8	0.70	0.69	0.78
6/6 Door	31.6	C	0.391	0.613	1.26 ± 0.17	94	27	18	0.73	0.66	0.89
6/6 Door	105.3	C	0.590	0.558	1.20 ± 0.23	207	38	14	0.75	0.72	0.87
6/6 Door	158.0	C	0.657	0.539	1.20 ± 0.23	289	56	16	0.75	0.70	0.87
6/6 Door	62.9	AR[a]	0.522	0.593	1.26 ± 0.17	136	21	6	0.73	0.70	0.96
6/6 Door	62.9	BR	0.467	0.555	1.49 ± 0.17	190	25	6	0.73	0.70	1.04
6/6 Door	62.9	CR	0.483	0.566	1.37 ± 0.17	161	24	7	0.73	0.69	0.93
6/6 Door	62.9	DR	0.478	0.565	1.49 ± 0.17	153	27	6	0.70	0.69	0.92
6/6 Door	62.9	ER	0.497	0.581	1.26 ± 0.17	149	21	6	0.75	0.71	0.99
6/6 Door	62.9	FR	0.541	0.588	1.14 ± 0.17	129	24	7	0.69	0.65	0.87
6/6 Door	62.9	GR	0.575	0.580	1.09 ± 0.23	117	28	7	0.72	0.63	0.87
6/6 Door	62.9	HR	0.483	0.597	1.26 ± 0.17	150	19	7	0.71	0.71	0.93

[a] R denotes "raised" burner

Table 1 (continued)

Opening Configuration (Fig. 3)	Fire Strength Q (kW)	Fire Location (Fig. 2)	Air Mass Flow Rate $\dot{m}_a$ (kg/s)	Neutral Plane Location N/H_o	Thermal Interface Height Z_d (m)	Avg. Temp. of Upper Gas Layer T_{gu} (°C)	Avg. Temp. of Lower Gas Layer $T_{g\ell}$ (°C)	Ambient Temperature T_a (°C)	Method A C_o	Method A C_1	Method B C_o
2/6 Door	30.2	ℓ[b] = 0.46 m	0.171	0.588	1.14 ± 0.17	138	50	26	0.72	0.69	0.77
4/6 Door	30.3	ℓ = 0.46 m	0.290	0.568	1.31 ± 0.11	116	41	26	0.75	0.71	0.85
6/6 Door	30.2	ℓ = 0.46 m	0.372	0.575	1.43 ± 0.11	113	42	28	0.74	0.68	0.90
8/6 Door	28.3	ℓ = 0.46 m	0.436	0.588	1.49 ± 0.17	105	37	27	0.76	0.65	0.98
2/6 Door	120.3	ℓ = 1.83 m	0.267	0.487	0.80 ± 0.17	324	132	31	0.73	0.69	0.74
4/6 Door	120.4	ℓ = 1.83 m	0.484	0.530	1.03 ± 0.17	231	80	30	0.76	0.73	0.79
6/6 Door	120.0	ℓ = 1.83 m	0.622	0.553	1.14 ± 0.17	206	71	32	0.74	0.68	0.82
8/6 Door	120.1	ℓ = 1.83 m	0.741	0.576	1.20 ± 0.23	184	58	32	0.75	0.67	0.88

[b] ℓ is length of line burner

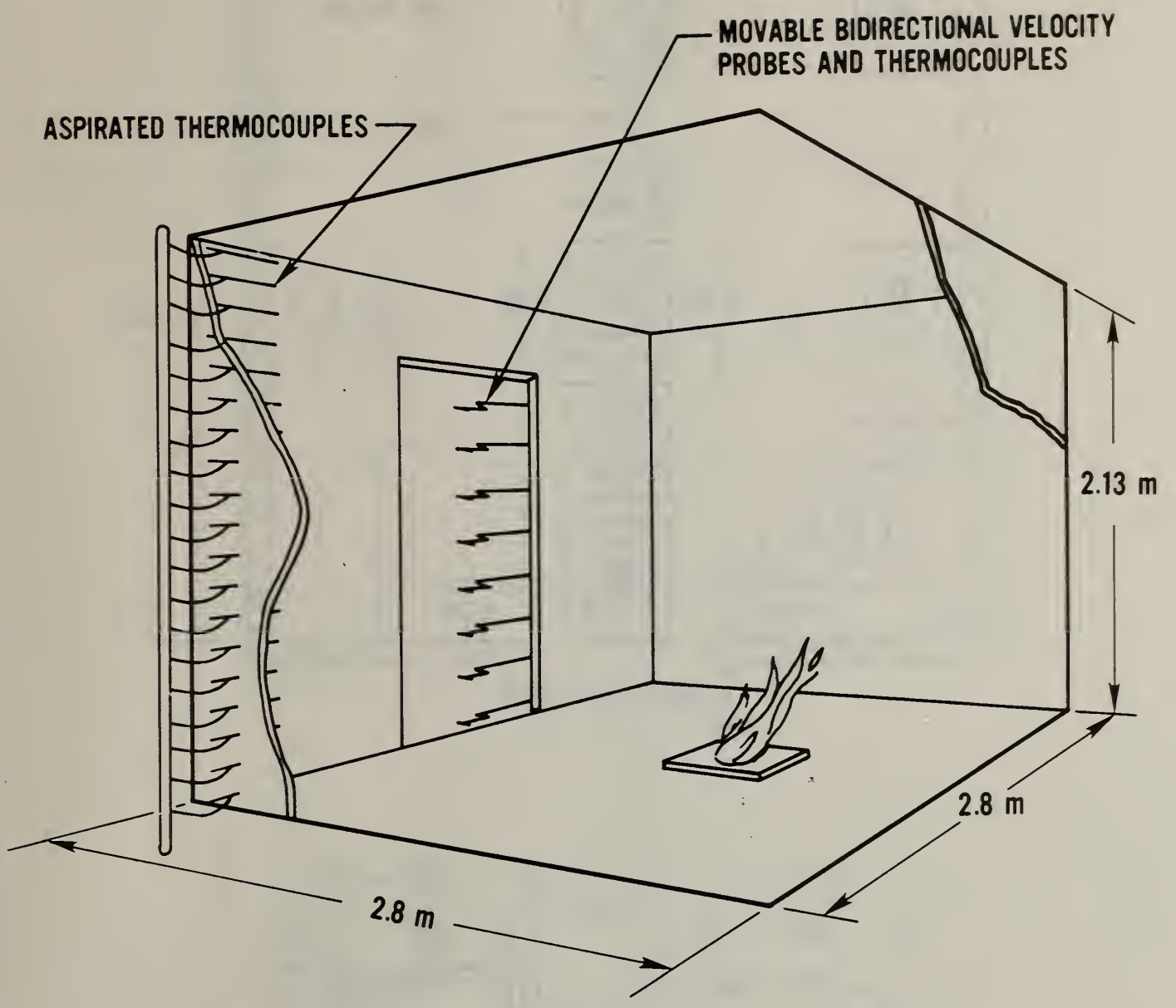

Fig. 1. Test room.

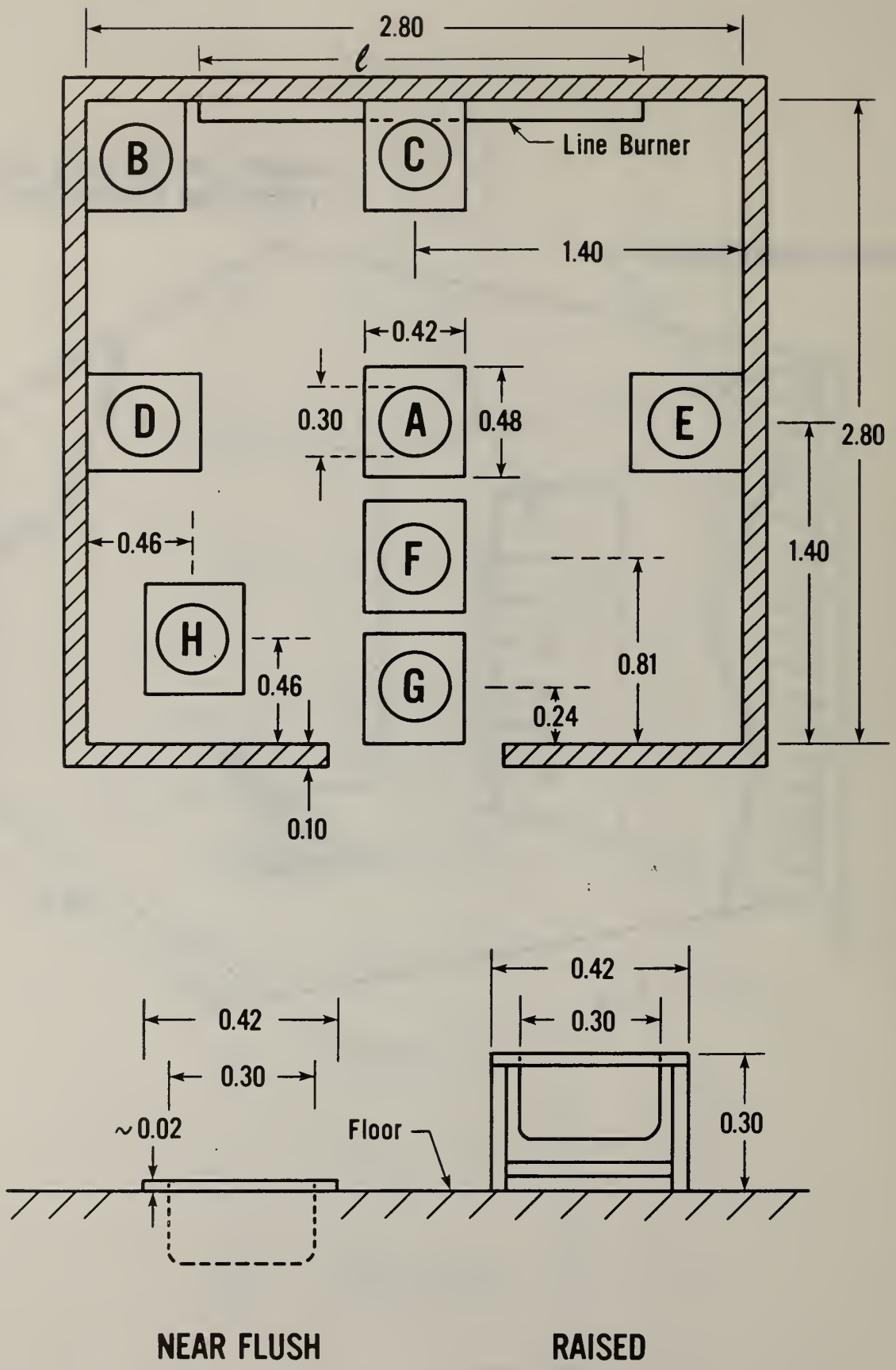

Fig. 2. Gas burner locations with dimensions in meters.

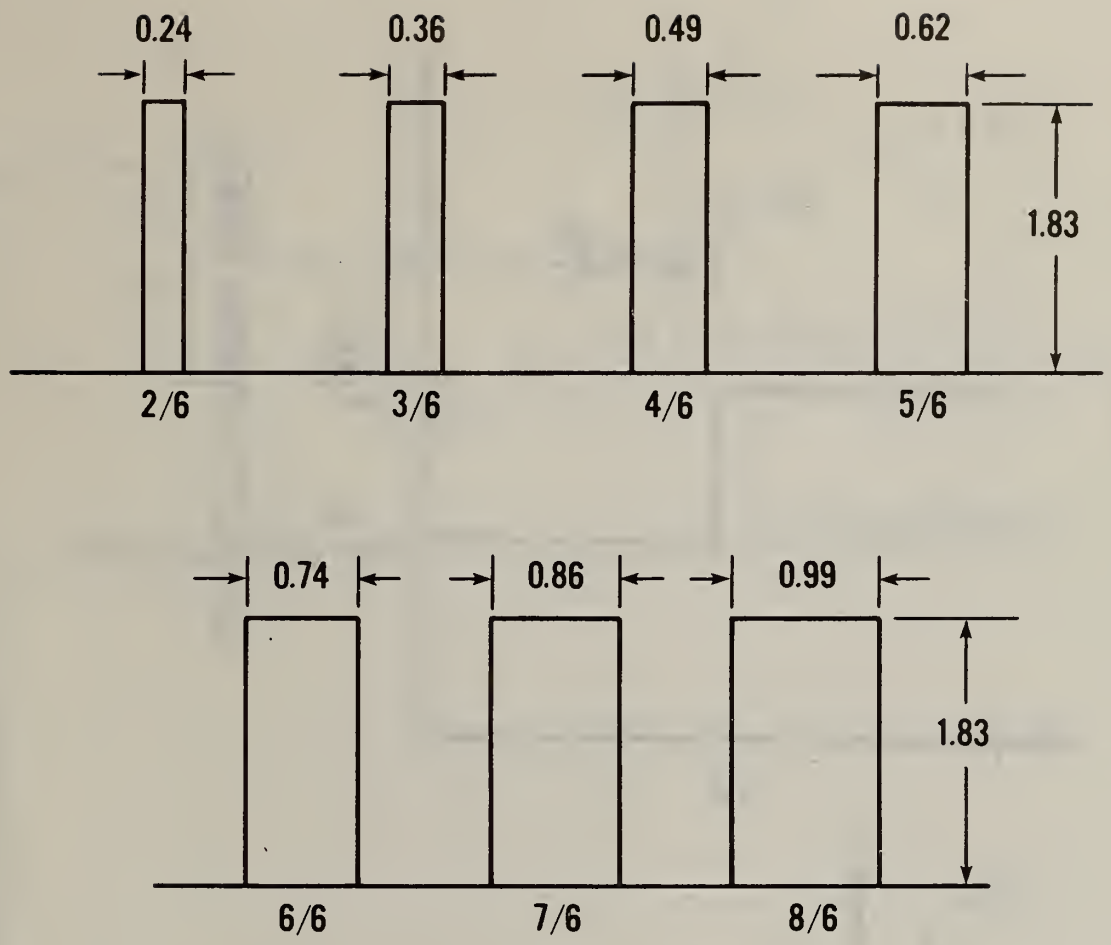

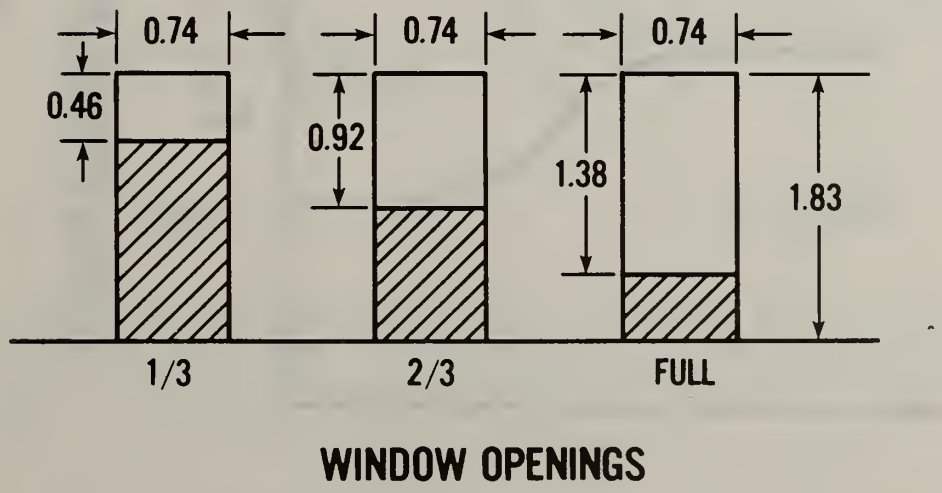

Fig. 3. Room opening configurations with dimensions in meters.

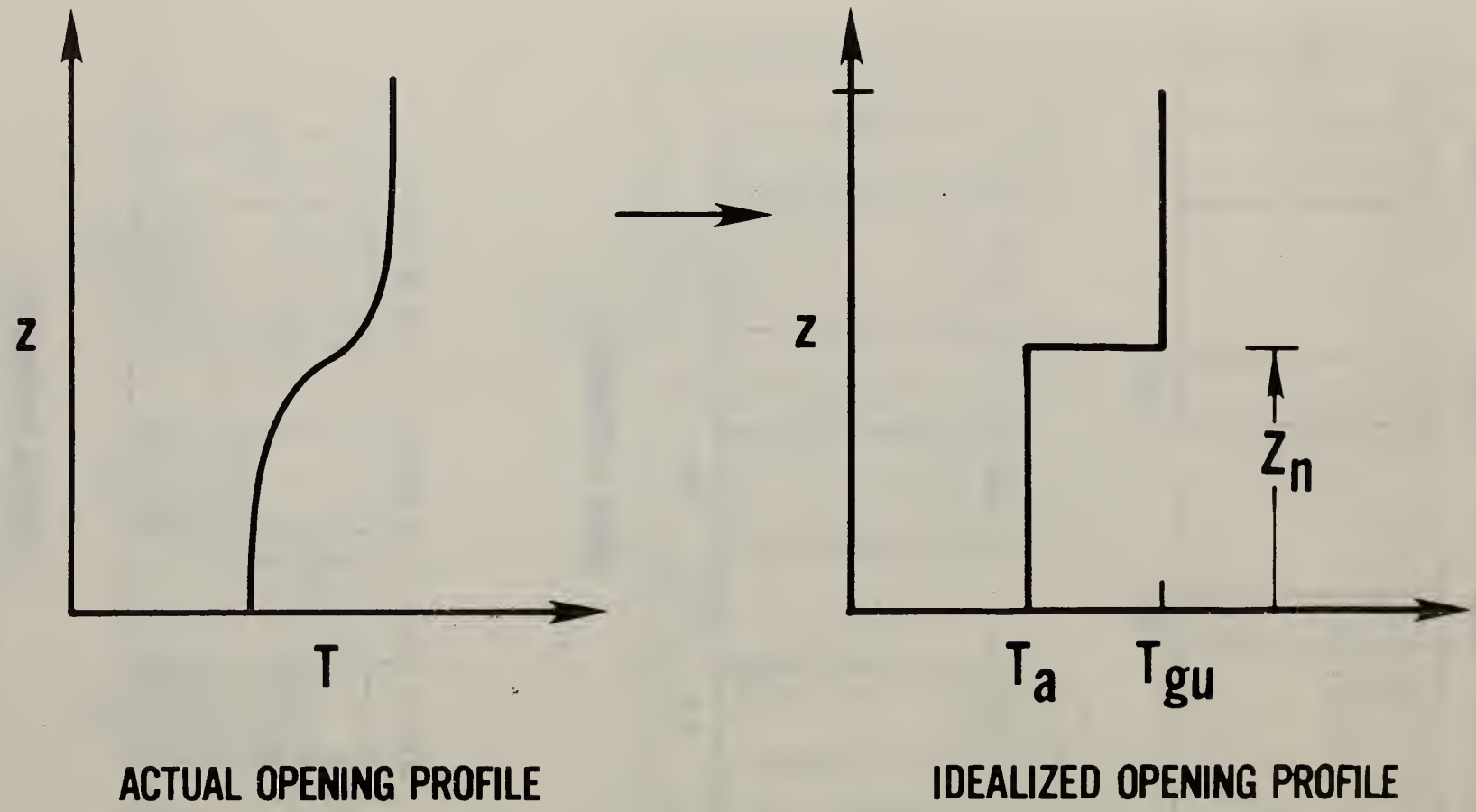

Fig. 4. Two-layer approximation of opening temperature profile.

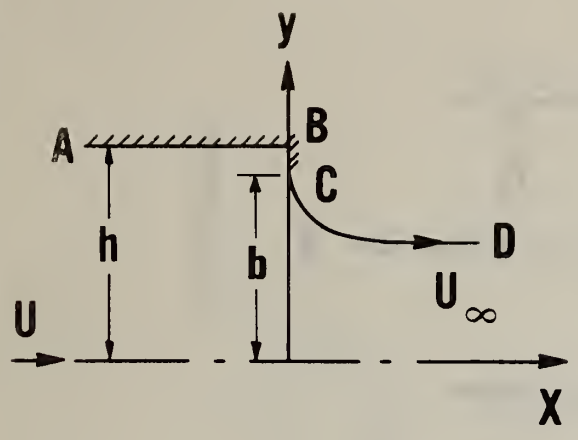

a. Physical plane

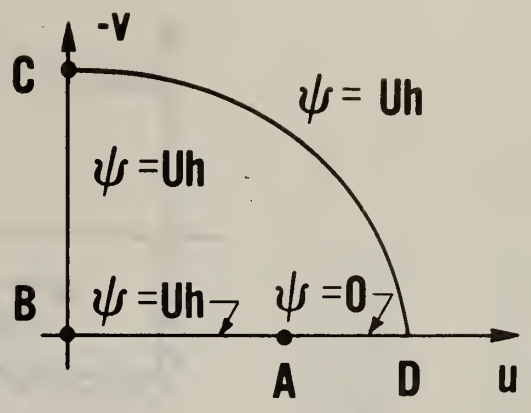

b. Hodograph plane

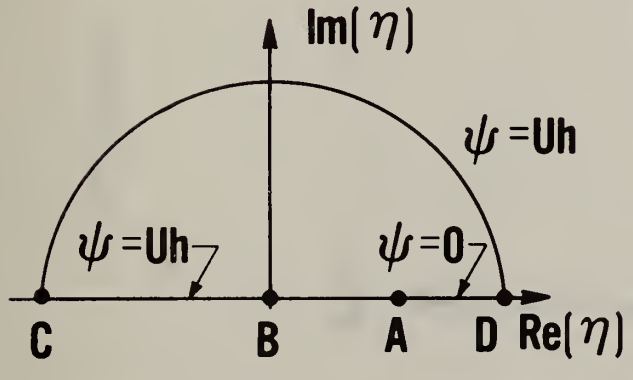

c. η - plane

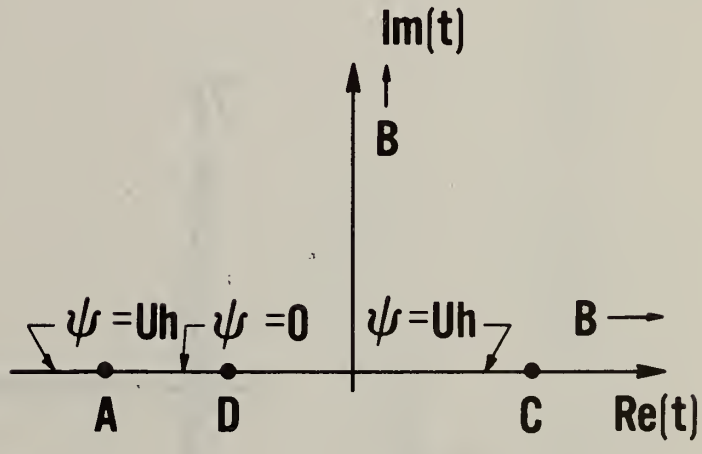

d. t-plane

Fig. 5. Transformations showing mappings from physical plane (a), to hodograph plane (b), to η plane (c), to t plane (d). The point B is at infinity in the t plane. The coordinates of points A, D, and C in the t plane are $-(U^2 + U_\infty^4/U^2)$, $-2U_\infty^2$, and $2U_\infty^2$ respectively.

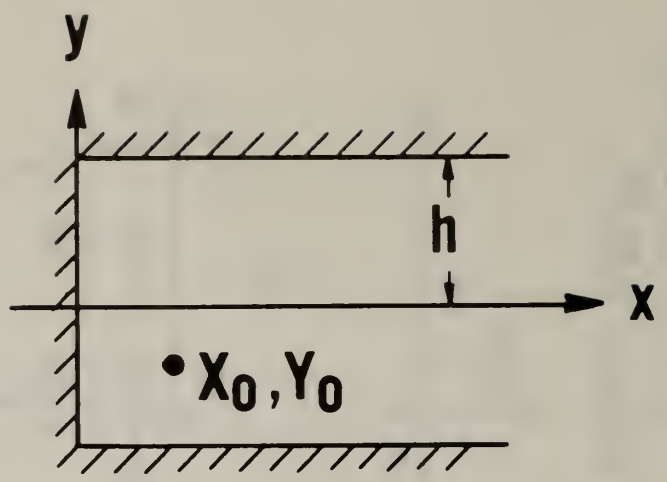

a. Physical plane

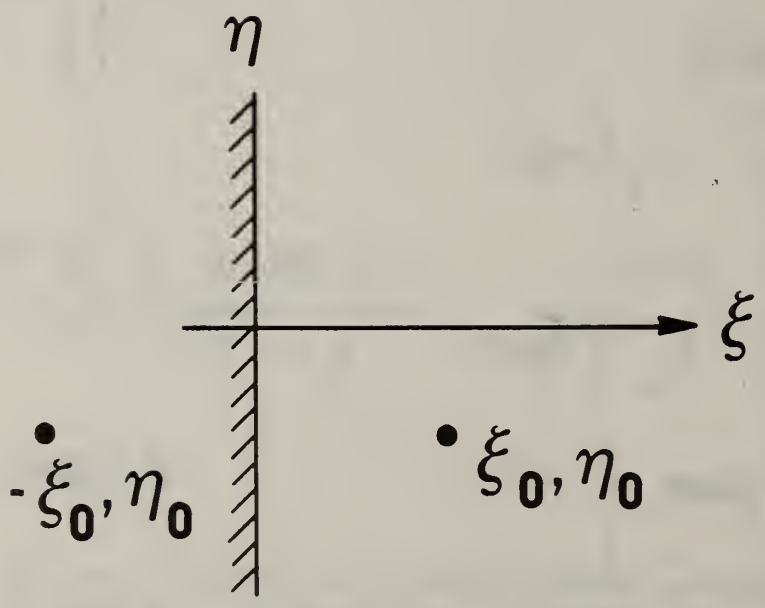

b. ζ - plane

Fig. 6. Transformation showing mapping of plan view of enclosure from physical plane (a) to hodograph plane (b). The source representing the plume is at x_o, y_o.

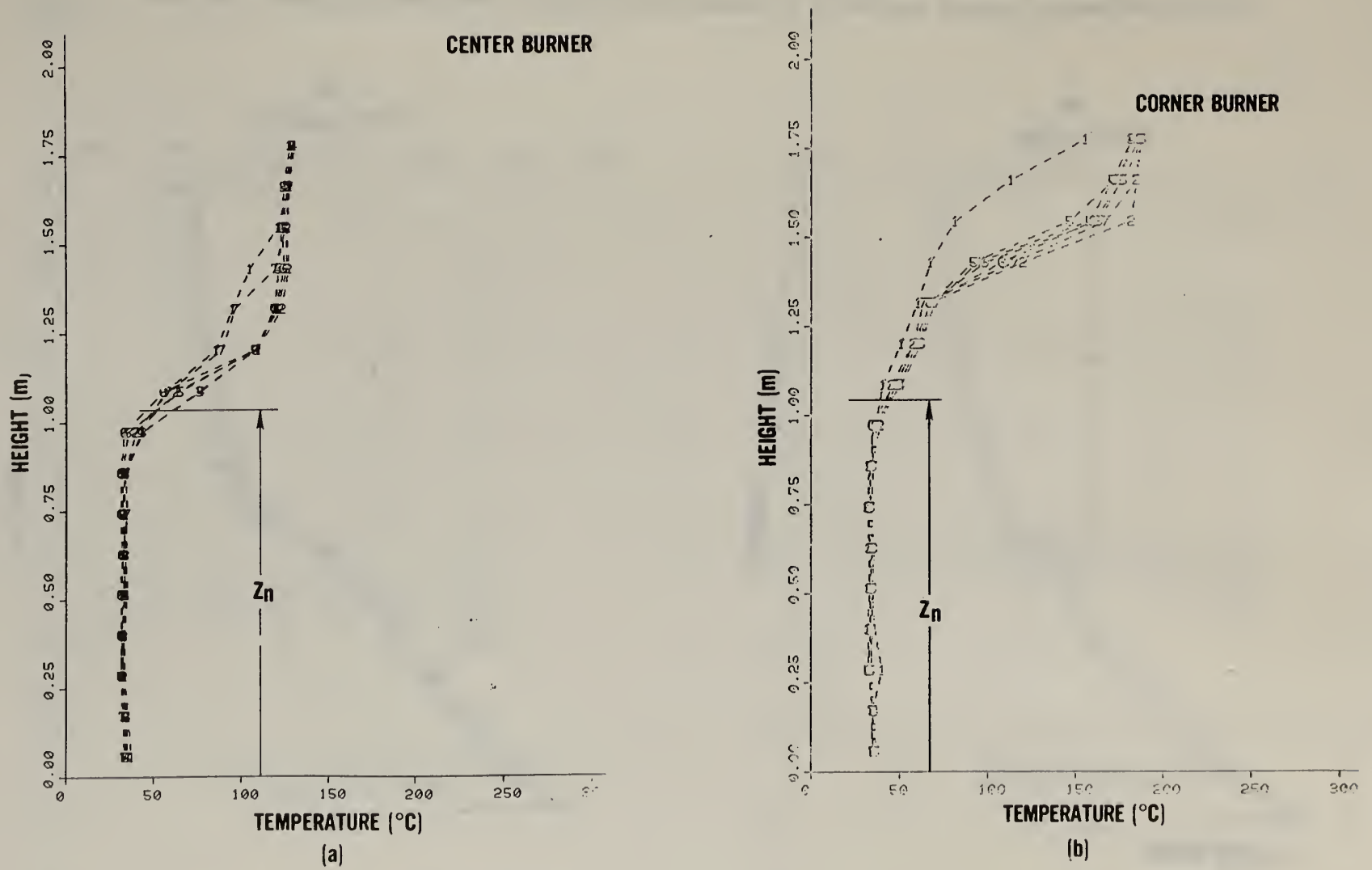

Fig. 7. Vertical temperature profiles at different horizontal locations within doorway; H_o = 1.829 m, W_o = 0.737 m, $\dot{Q}$ = 63 kW; (a) center burner, (b) corner burner.

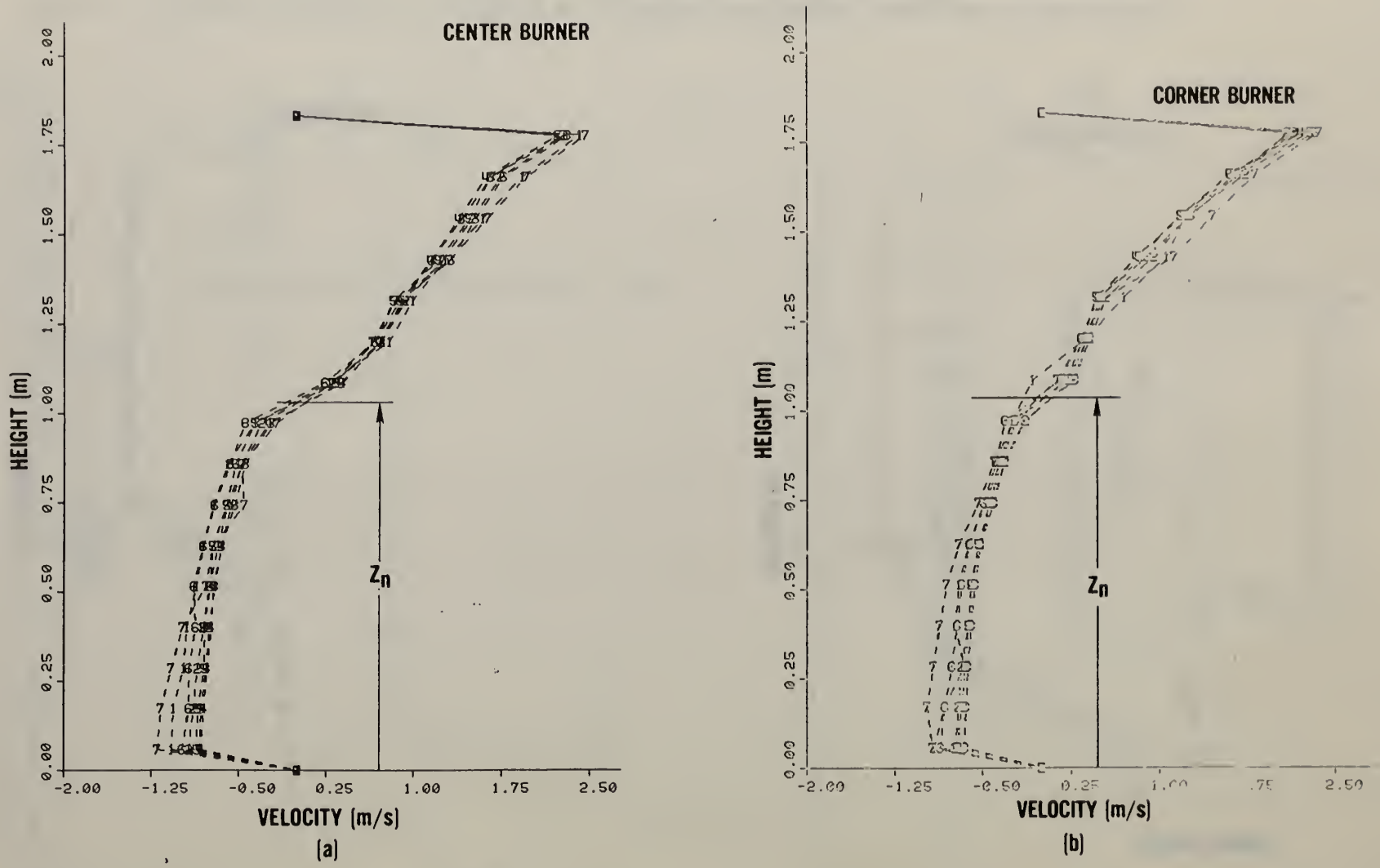

Fig. 8. Vertical velocity profiles at different horizontal locations within doorway; H_o = 1.829 m, W_o = 0.737 m, $\dot{Q}$ = 63 kW; (a) center burner, (b) corner burner.

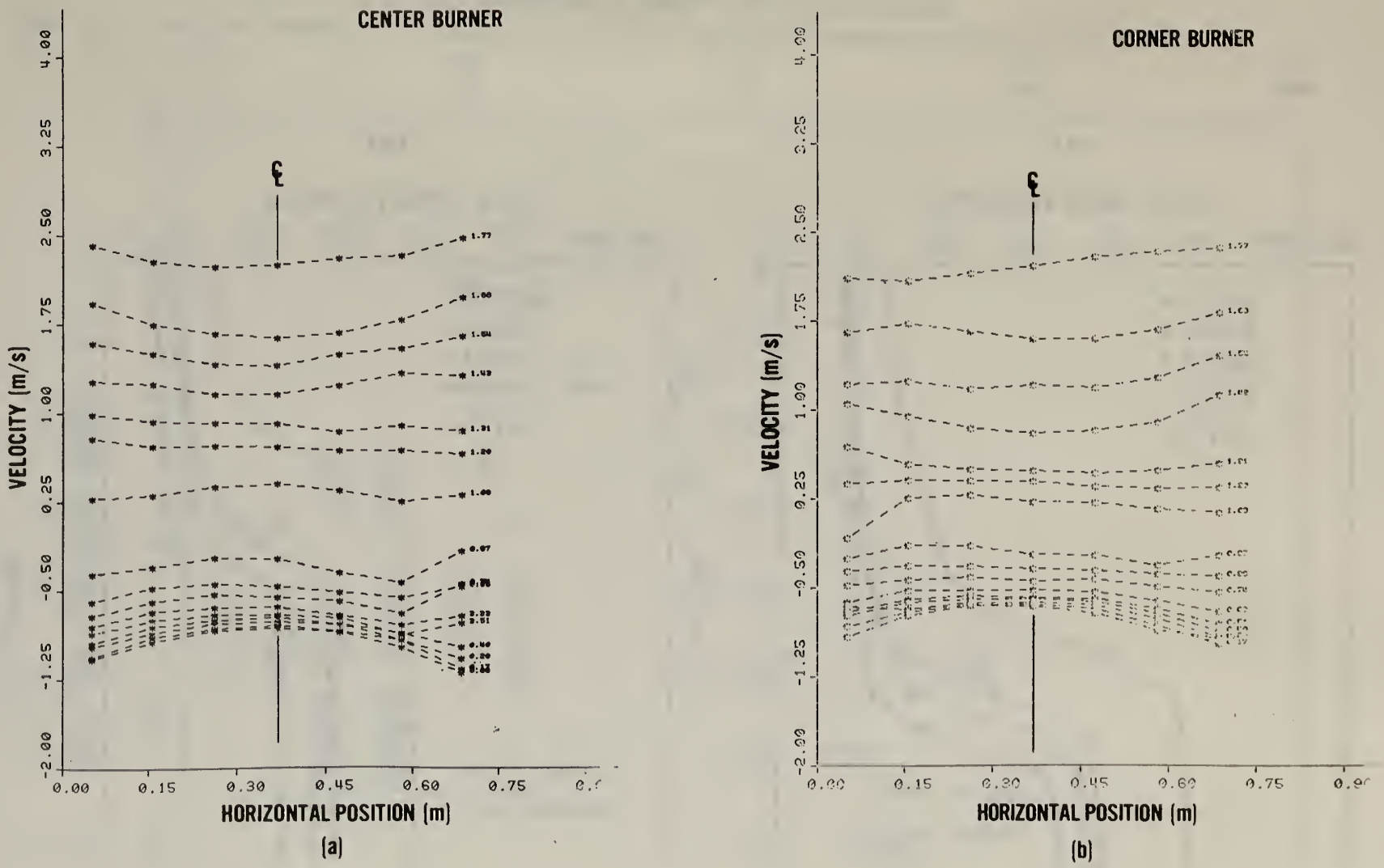

Fig. 9. Horizontal velocity profiles at different vertical locations within doorway; H_o = 1.829 m, W_o = 0.737 m, Q = 63 kW; (a) center burner, (b) corner burner. Horizontal distance is measured from the left side of the jamb as viewed from outside the room.

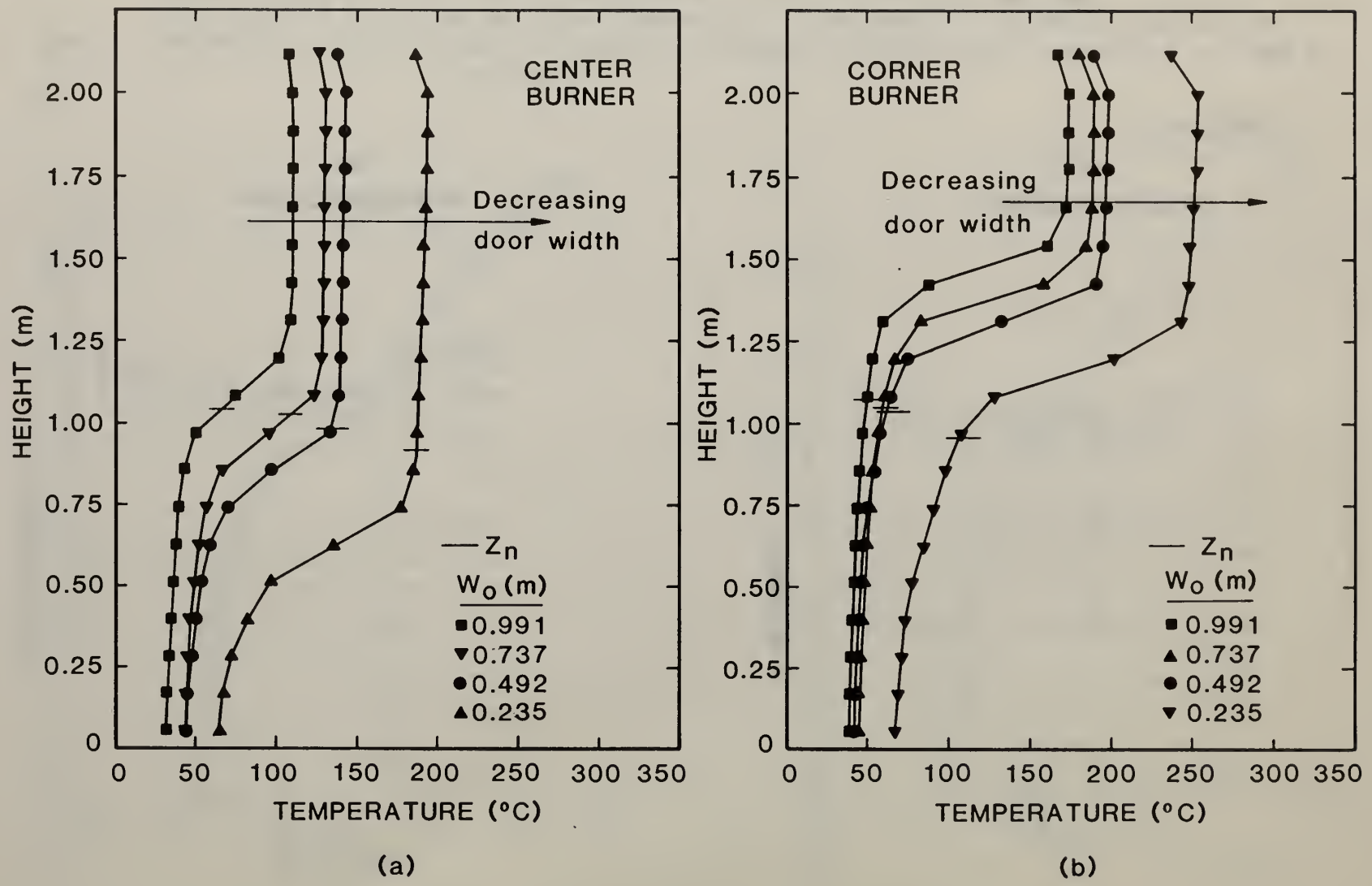

Fig. 10. Vertical temperature profiles measured by aspirated thermocouples in test room; H_o = 1.829 m, $\dot{Q}$ = 63 kW; (a) center burner, (b) corner burner.

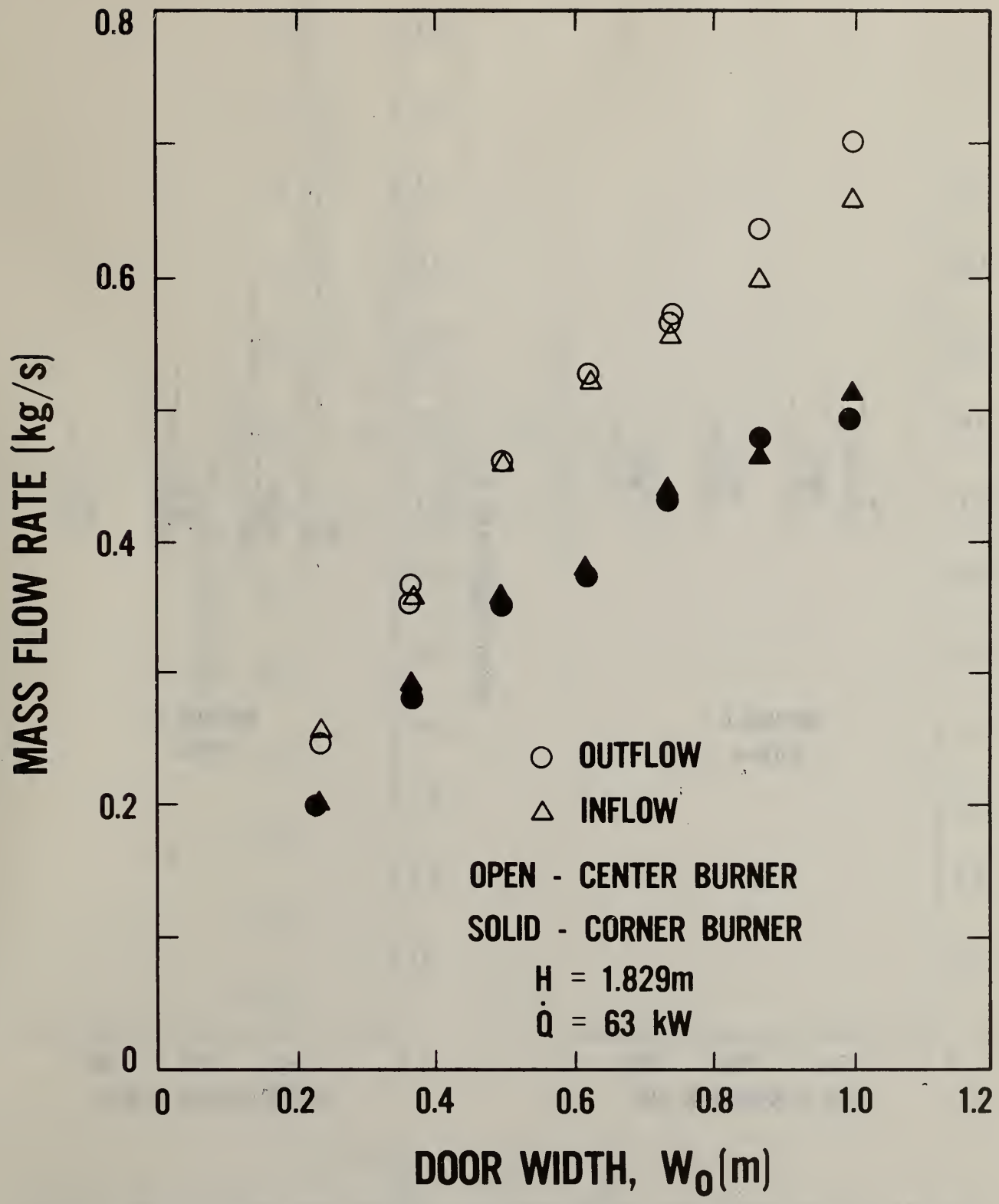

Fig. 11. Mass flow rate vs. door width for fixed fire strength and door height.

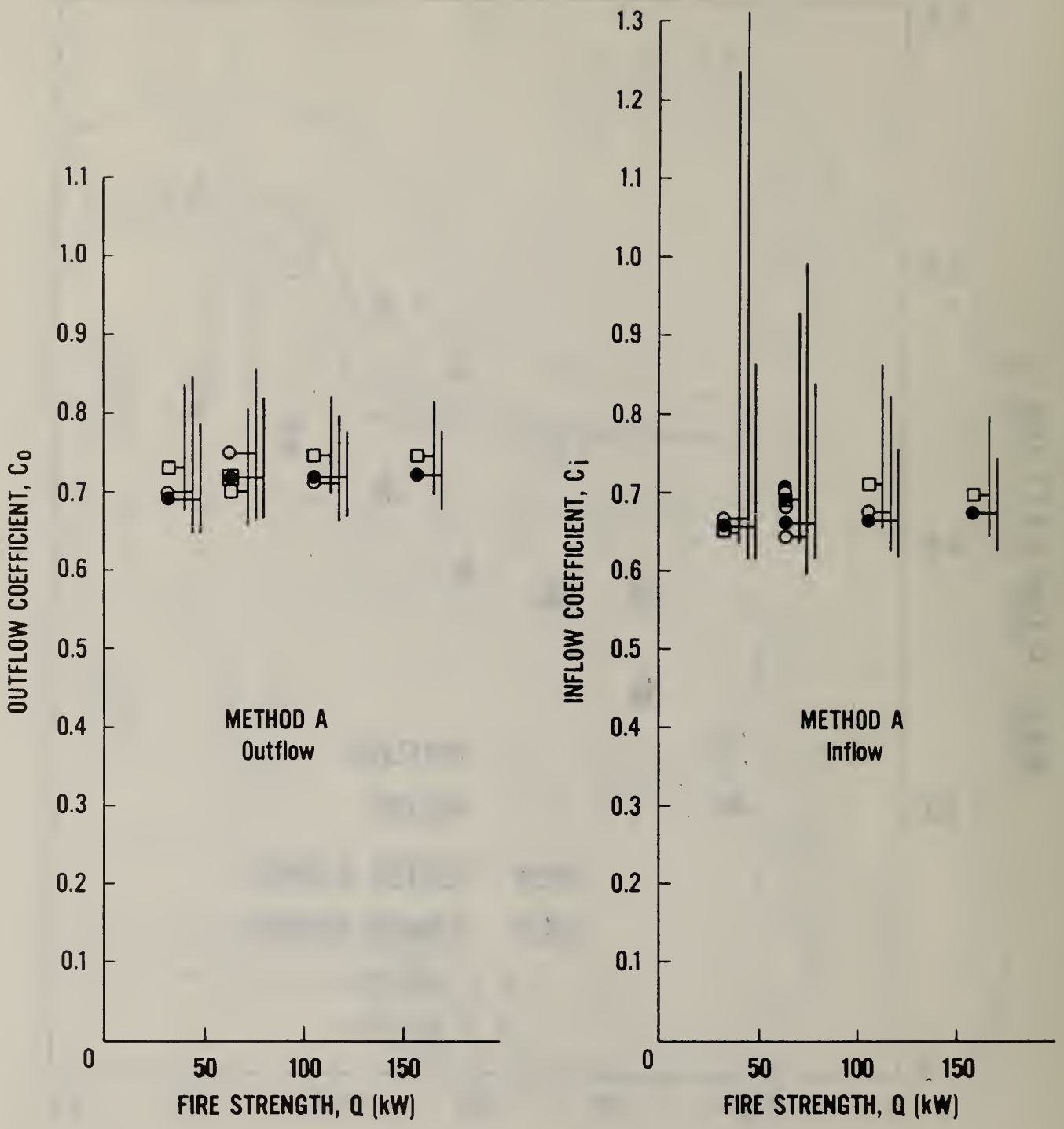

Fig. 12. Flow coefficients by Method A for a fixed door (0.74 x 1.83 m high) as a function of fire strength.

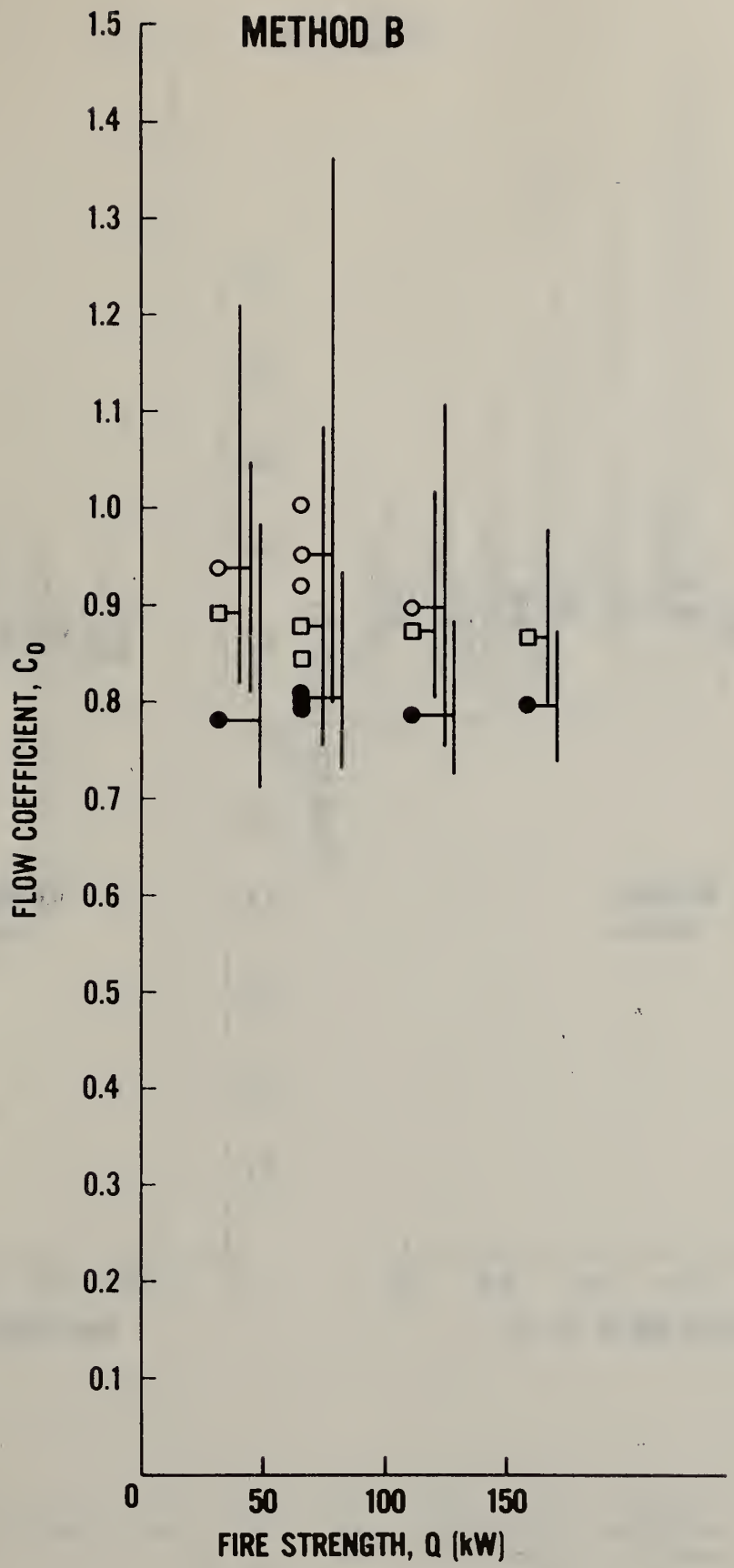

Fig. 13. Outflow coefficients by Method B for a fixed doorway (0.74 x 1.83 m high) as a function of fire strength.

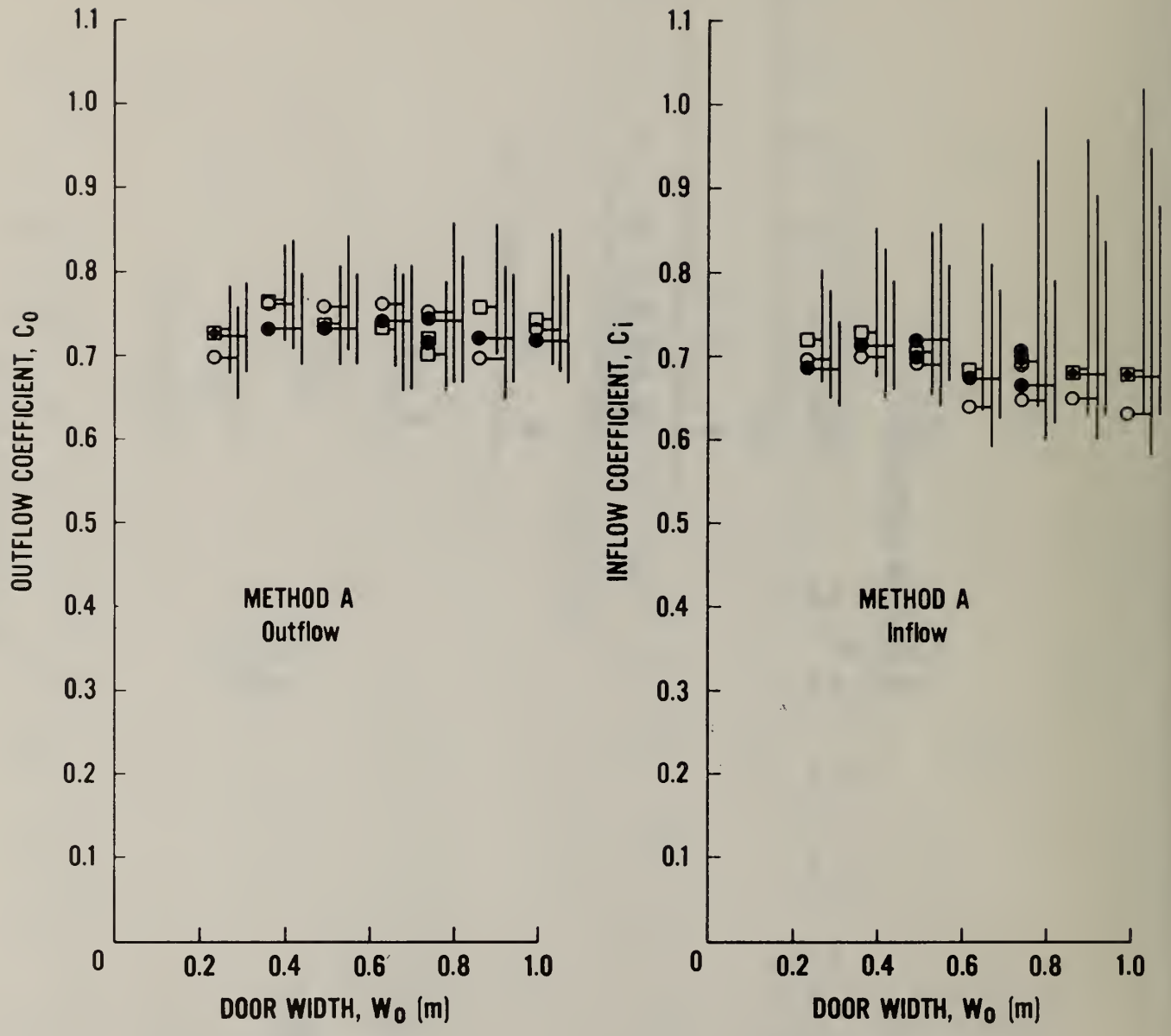

Fig. 14. Flow coefficients by Method A for $\dot{Q}$ = 63 kW as a function of door width, H_o = 1.83 m.

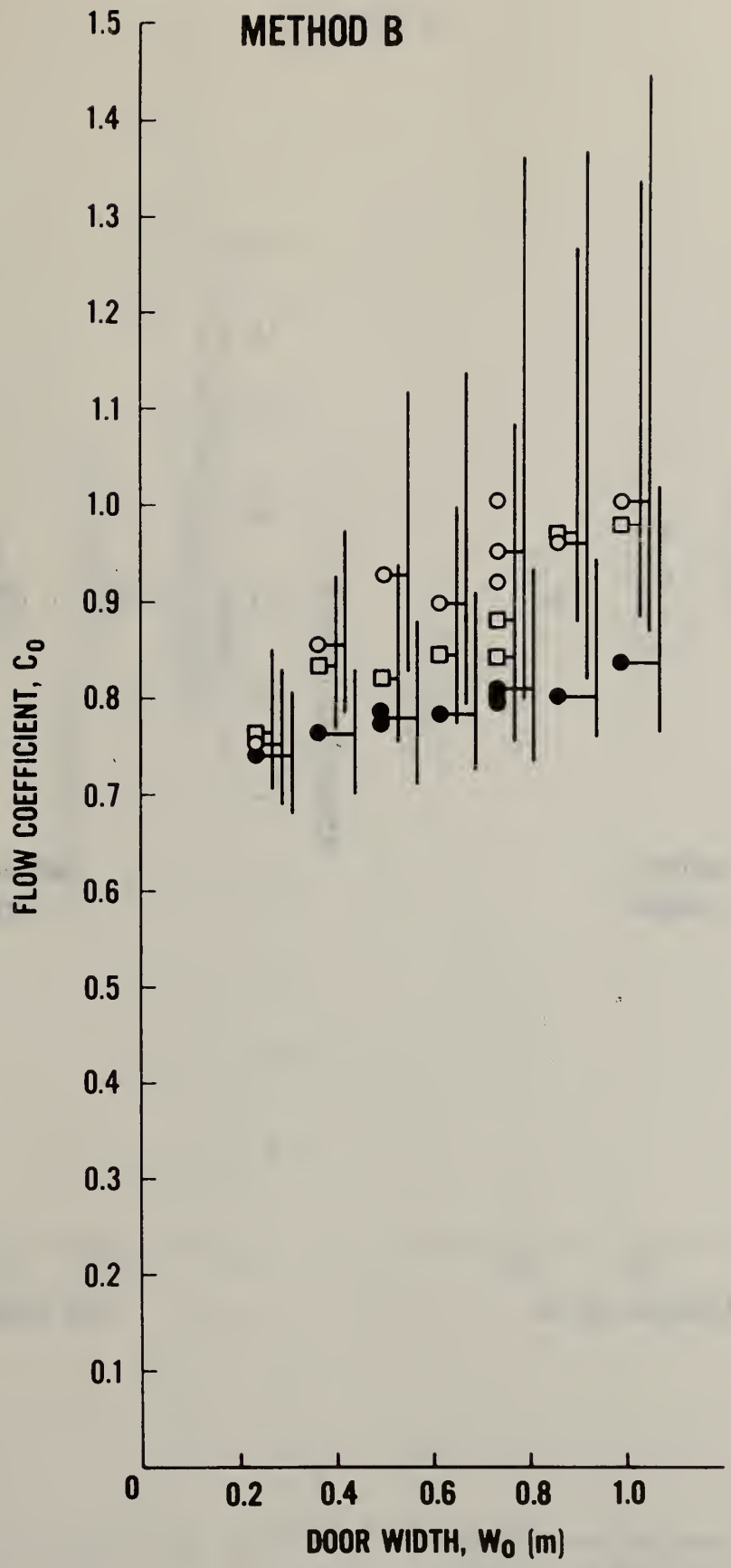

Fig. 15. Flow coefficients by Method B for $\dot{Q}$ = 63 kW as a function of door width, H_o = 1.83 m.

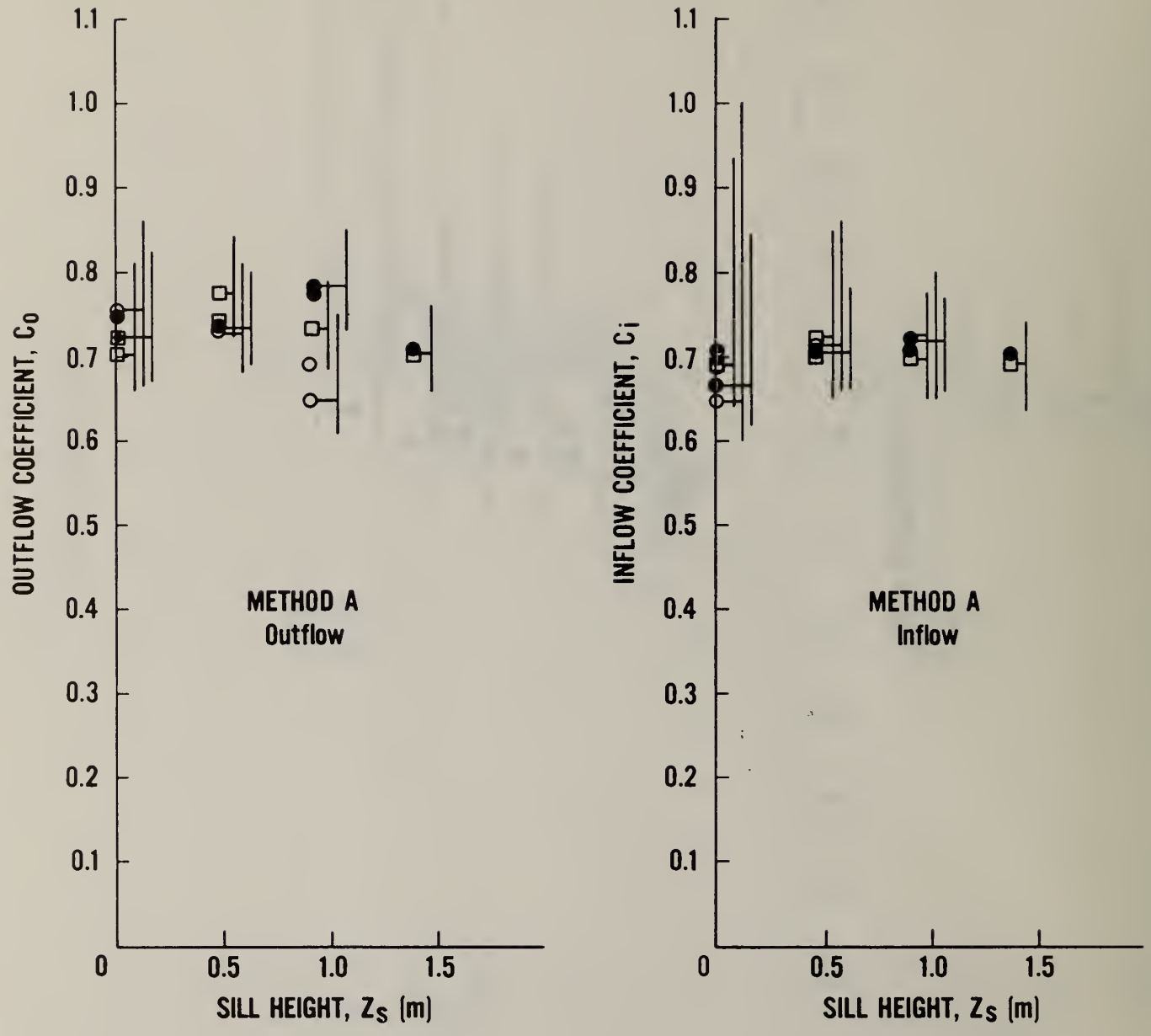

Fig. 16. Flow coefficients by Method A as a function of window size for $\dot{Q}$ = 63 kW and W_o = 0.73 m.

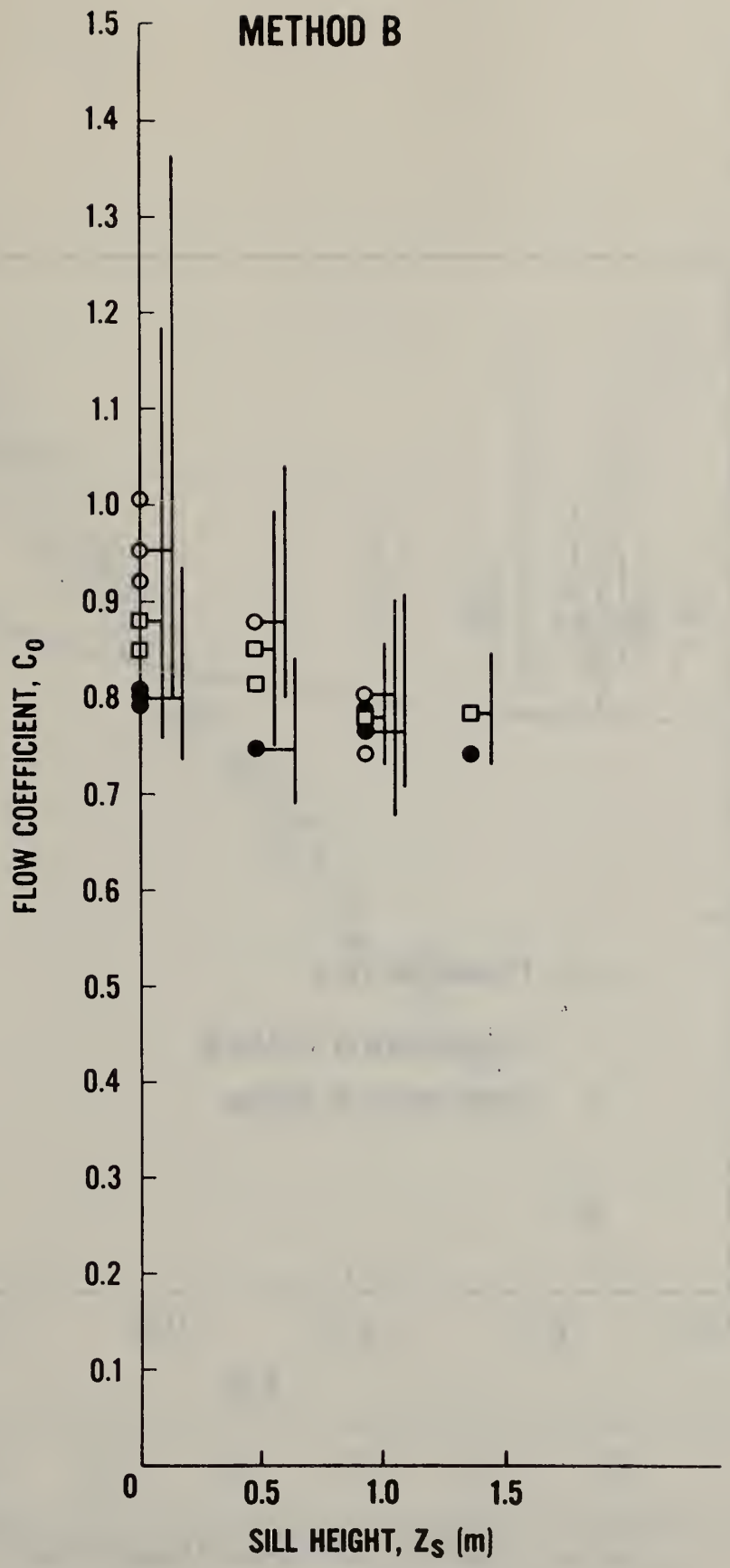

Fig. 17. Outflow coefficients by Method B as a function of window size for $\dot{Q}$ = 63 kW and W_o = 0.73 m.

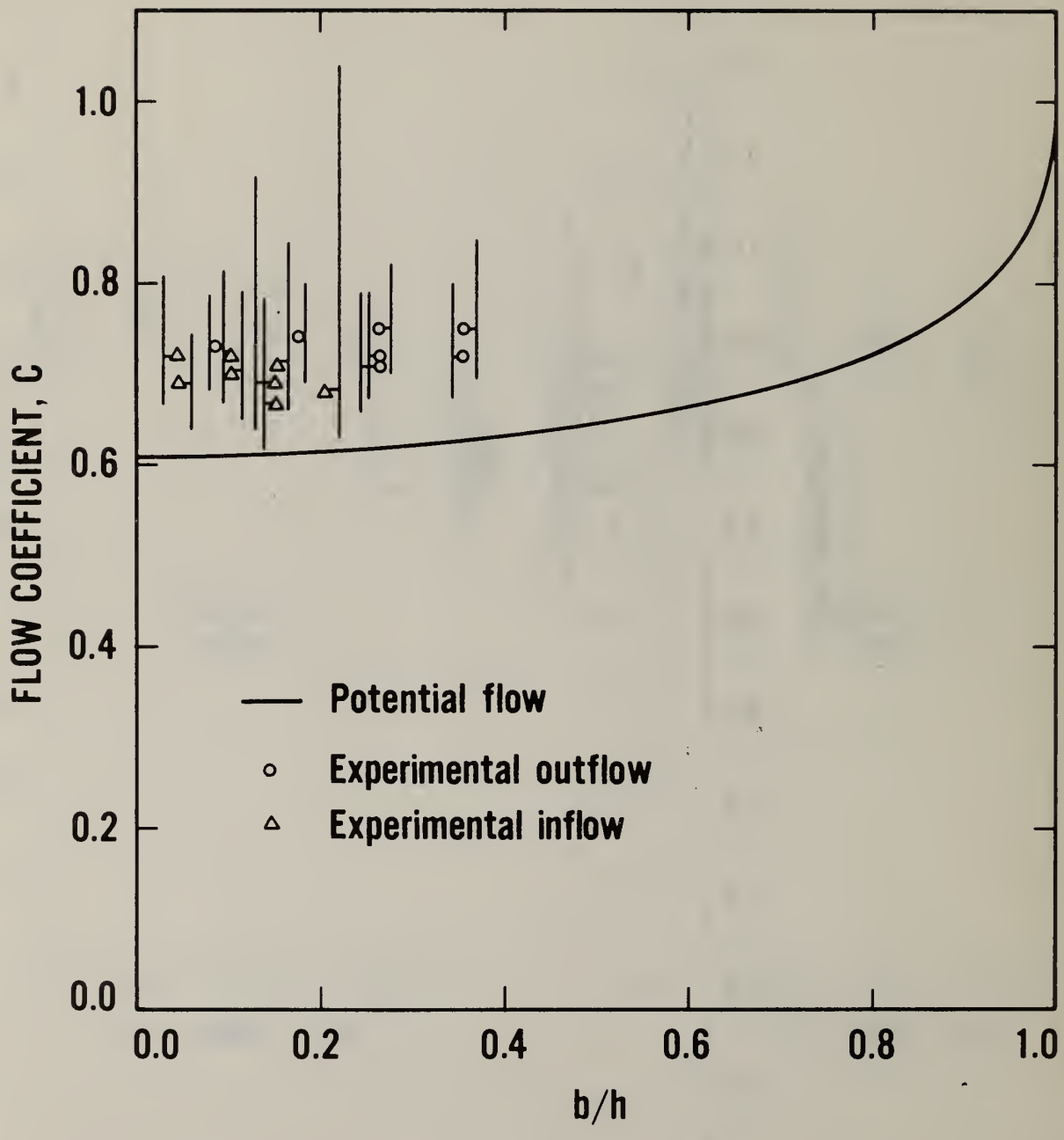

Fig. 18. Theoretical orifice coefficient C plotted as function of opening to room width ratio b/h. The experimental data obtained by Method A is replotted above.

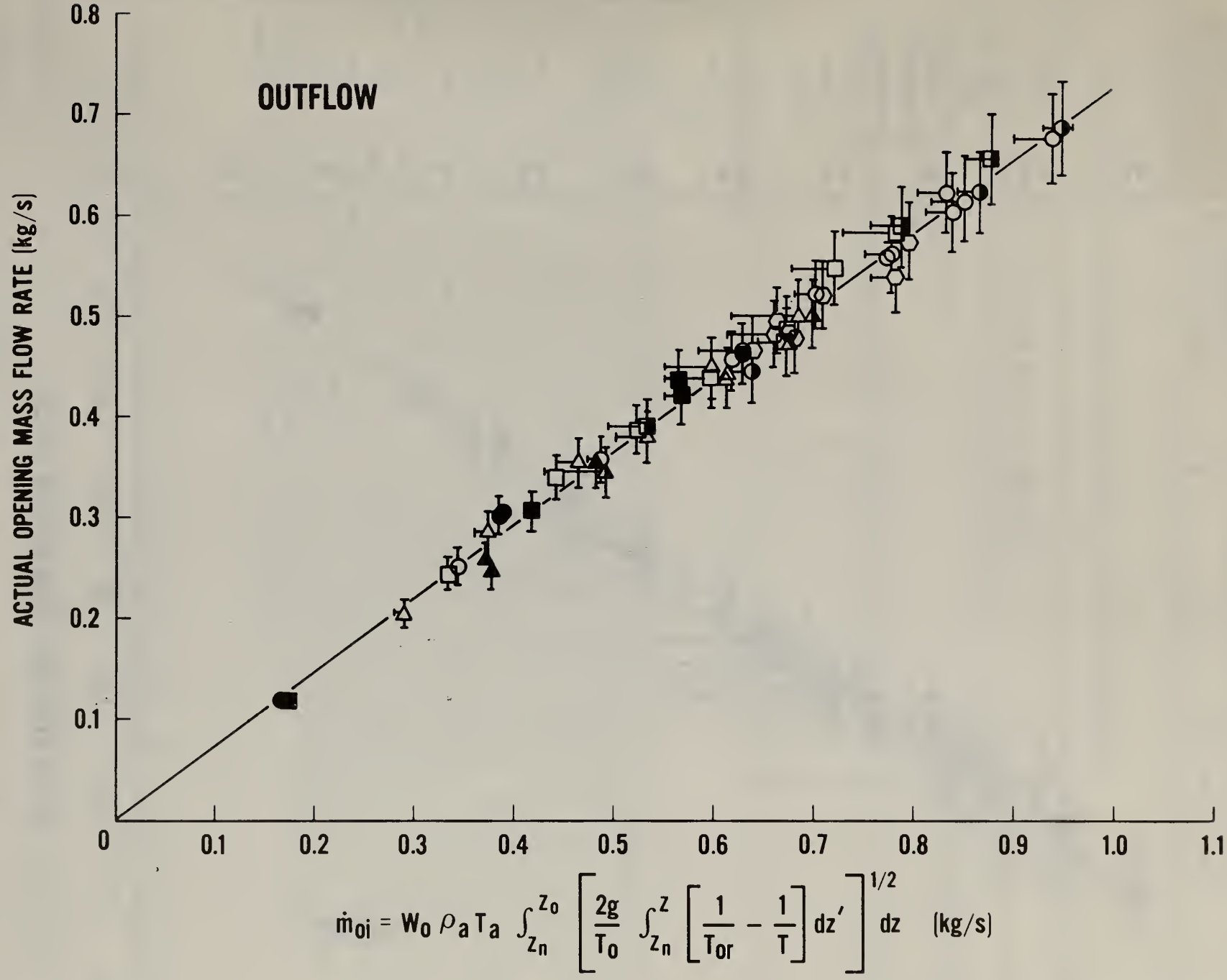

Fig. 19. Mass outflow rates predicted from temperatures.

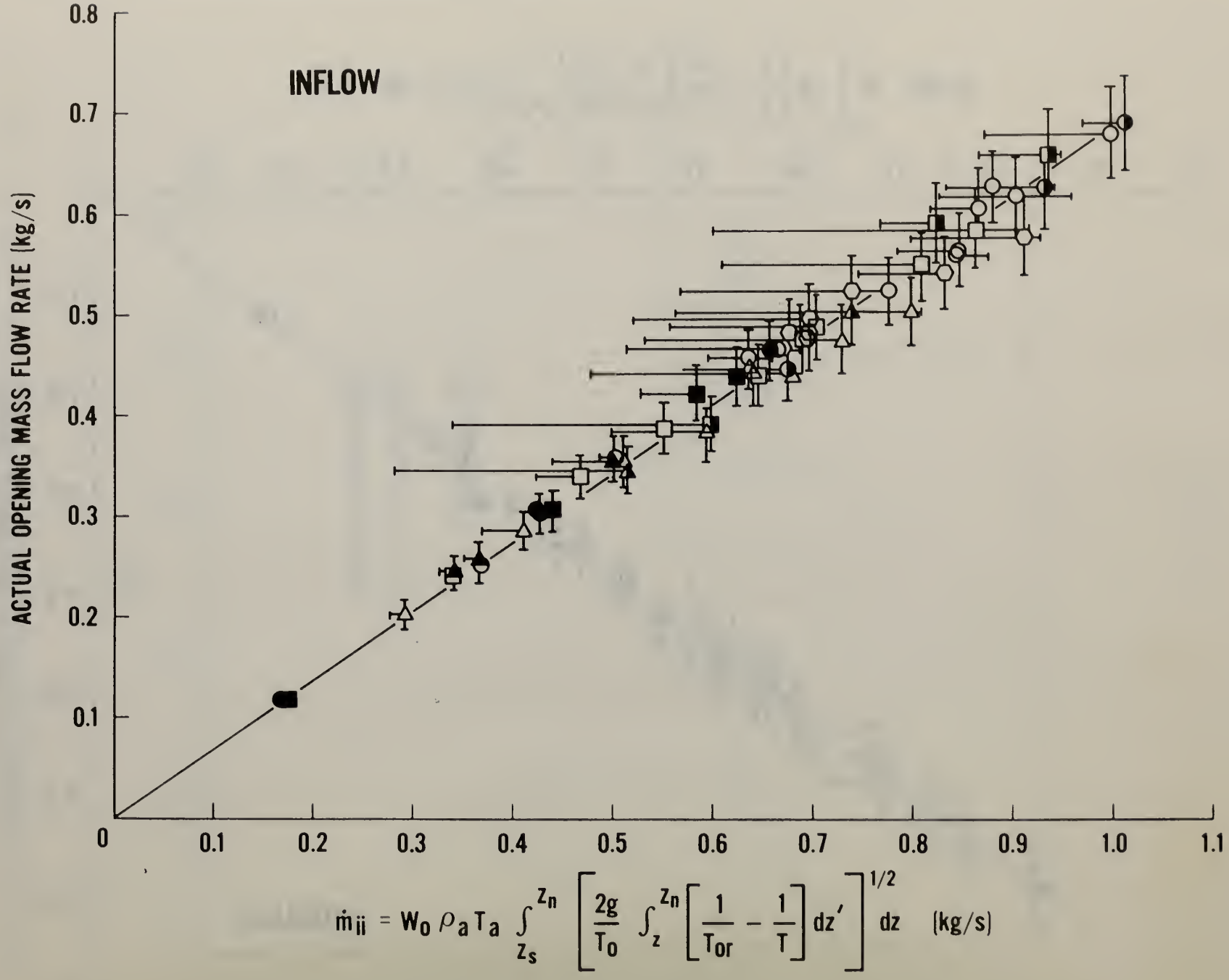

Fig. 20. Mass inflow rates predicted from temperatures.

NBS-114A (REV. 2-80)

U.S. DEPT. OF COMM. BIBLIOGRAPHIC DATA SHEET (See instructions)	1. PUBLICATION OR REPORT NO. NBSIR 83-2801	2. Performing Organ. Report No.	3. Publication Date March 1984

4. TITLE AND SUBTITLE

Fire Induced Flows Through Room Openings - Flow Coefficients

5. AUTHOR(S)

K.D. Steckler, H.R. Baum and J.G. Quintiere

6. PERFORMING ORGANIZATION (If joint or other than NBS, see instructions)

NATIONAL BUREAU OF STANDARDS
DEPARTMENT OF COMMERCE
WASHINGTON, D.C. 20234

7. Contract/Grant No.

8. Type of Report & Period Covered

9. SPONSORING ORGANIZATION NAME AND COMPLETE ADDRESS (Street, City, State, ZIP)

10. SUPPLEMENTARY NOTES

☐ Document describes a computer program; SF-185, FIPS Software Summary, is attached.

11. ABSTRACT (A 200-word or less factual summary of most significant information. If document includes a significant bibliography or literature survey, mention it here)

A full-scale experimental and theoretical study was made of steady-state fire-induced flows through doorway and window openings. Measurements included two-dimensional temperature and pressure-difference profiles within the opening and vertical temperature profiles within the rooms connected by the openings. A floor-level gas burner served as the energy source. Mass flow rates through the openings were calculated from the opening data. A static-pressure flow model was used to establish ideal orifice flows from different combinations of the experimental temperature profiles. The opening and ideal flow results were combined to form room-opening flow coefficients as a function of fire energy release rate, opening geometry, and fire location. Two calculation procedures were used to compute the ideal flow. An irrotational jet model for the flow coefficients was developed and found to be in reasonable agreement with these and other measurements. Measured flow coefficient results show no significant dependence on fire strength, opening geometry, or fire location, as long as the ideal mass flow rate was based on measured gas temperatures. However, the theory indicates a significant variation in flow coefficient with opening widths larger than those used in the experiments.

12. KEY WORDS (Six to twelve entries; alphabetical order; capitalize only proper names; and separate key words by semicolons)

air flows; compartment fires; flow coefficients; opening flows; orifice coefficients

13. AVAILABILITY

☒ Unlimited

☐ For Official Distribution. Do Not Release to NTIS

☐ Order From Superintendent of Documents, U.S. Government Printing Office, Washington, D.C. 20402.

☒ Order From National Technical Information Service (NTIS), Springfield, VA. 22161

14. NO. OF PRINTED PAGES

59

15. Price

$10.00